ARTICLE

https://doi.org/10.1038/s41586-018-0415-5

Modulating plant growth–metabolism coordination for sustainable agriculture

Shan Li[1,2], Yonghang Tian[1], Kun Wu[1], Yafeng Ye[1], Jianping Yu[1], Jianqing Zhang[1], Qian Liu[1], Mengyun Hu[3], Hui Li[3], Yiping Tong[1], Nicholas P. Harberd[4] & Xiangdong Fu[1,2]*

Enhancing global food security by increasing the productivity of green revolution varieties of cereals risks increasing the collateral environmental damage produced by inorganic nitrogen fertilizers. Improvements in the efficiency of nitrogen use of crops are therefore essential; however, they require an in-depth understanding of the co-regulatory mechanisms that integrate growth, nitrogen assimilation and carbon fixation. Here we show that the balanced opposing activities and physical interactions of the rice GROWTH-REGULATING FACTOR 4 (GRF4) transcription factor and the growth inhibitor DELLA confer homeostatic co-regulation of growth and the metabolism of carbon and nitrogen. GRF4 promotes and integrates nitrogen assimilation, carbon fixation and growth, whereas DELLA inhibits these processes. As a consequence, the accumulation of DELLA that is characteristic of green revolution varieties confers not only yield-enhancing dwarfism, but also reduces the efficiency of nitrogen use. However, the nitrogen-use efficiency of green revolution varieties and grain yield are increased by tipping the GRF4–DELLA balance towards increased GRF4 abundance. Modulation of plant growth and metabolic co-regulation thus enables novel breeding strategies for future sustainable food security and a new green revolution.

The green revolution of the 1960s boosted crop yields, and was partly driven by widespread adoption of semi-dwarf green revolution varieties of cereals (GRVs)[1–4]. GRV semi-dwarfism is due to the accumulation of growth-repressing DELLA proteins (DELLAs) conferred by mutant alleles at the *Rht* (wheat)[5,6] and *SD1* (rice)[7,8] loci. In normal plants, gibberellin (GA) promotes growth by stimulating the destruction of DELLAs[9,10]. Mutant wheat GRV DELLAs[5] are resistant to GA-stimulated destruction, whereas the rice GRV mutant *sd1* allele reduces bioactive GA abundance[11,12], thus increasing accumulation of the DELLA protein SLR1 (Fig. 1a, b). The conferred semi-dwarfism causes GRV resistance to yield-reducing 'lodging' (flattening of plants by wind and rain)[4].

GRV lodging resistance is enhanced by relative insensitivity to nitrogen. For example, the nitrogen-induced increase in Nanjing6 (NJ6) plant height is reduced in NJ6-*sd1* (Fig. 1c), and the *Rht-B1b* GRV allele confers similar properties on wheat (Fig. 1d). Although DELLA accumulation inhibits GRV growth nitrogen response, nitrogen allocation to grain continues, thus combining enhanced harvestable yield with reduced lodging risk from increased nitrogen supply[1,4,5,7,8]. These properties drove the rapid spread of GRV cultivation over the past 50 years[3], and also ensured retention of semi-dwarfing alleles in current elite varieties[5,6,12]. However, GRVs are associated with reduced nitrogen-use efficiency (NUE)[13]. Accordingly, mutant *sd1* and *Rht* alleles inhibit nitrogen uptake. For example, ammonium (NH_4^+) is the majority nitrogen source for anaerobic paddy-field rice roots[14]. Although NJ6 $^{15}NH_4^+$ uptake is regulated by nitrogen (the uptake rate is reduced by increasing nitrogen supply), *sd1* reduces the underlying NJ6-*sd1* uptake rate, and also interferes with its nitrogen-responsive regulation (Fig. 1e). Similarly, with nitrate (NO_3^-) being the majority nitrogen source in aerobic soils[15], the mutant *Rht-B1b* allele affects both underlying and nitrogen-regulated $^{15}NO_3^-$ uptake in wheat (Fig. 1f). Thus, DELLA accumulation confers combined semi-dwarfism, reduced growth nitrogen response and reduced nitrogen uptake to GRVs. In consequence, achievement of high GRV yield requires environmentally damaging nitrogen fertilizer inputs[16]. Development of new GRVs that combine high yields with reduced nitrogen supply is thus an urgent goal for global sustainable agriculture[2,17]. We therefore analysed GRV growth–metabolism integration, reasoning that our discoveries might in turn enable development of new GRVs with improved NUE.

GRF4 promotes rice GRV ammonium uptake

We found approximately threefold variation in the $^{15}NH_4^+$ uptake rates of 36 *sd1*-containing *indica* rice varieties and the *SD1*-containing NJ6 control (Fig. 2a), then crossed NM73 (having the highest rate; Fig. 2a) with NJ6 (recurrent parent) to generate a BC_1F_2 population. Quantitative trait locus (QTL) analysis of $^{15}NH_4^+$ uptake rates revealed two logarithm of odds (LOD)-score peaks (quantitative trait loci *NGR1* and *NGR2* (*qNGR*1 and *qNGR2*), Fig. 2b; Supplementary Table 1). Although the NM73 *qngr1* allele coincides in map position with *sd1*[7,8], the molecular identity of the NM73 *qngr2* allele, which was associated with increased $^{15}NH_4^+$ uptake rates, was unknown. Positional mapping localized *qngr2* to *GRF4*[18–20] (Extended Data Fig. 1a), suggesting a previously unknown function in NH_4^+ uptake regulation. Because a NM73 ($GRF4^{ngr2}$) allele heterozygote has a higher rate than a NJ6 ($GRF4^{NGR2}$) allele homozygote (Extended Data Fig. 1b), $GRF4^{ngr2}$ semi-dominantly increases NH_4^+ uptakes. An NJ6-$GRF4^{ngr2}$ isogenic line accordingly exhibited increased NH_4^+ uptake rates (versus NJ6; Fig. 2c), and increased *GRF4* mRNA and GRF4 protein abundances (Fig. 2d, Extended Data Fig. 1c). Furthermore, RNA interference targeting *GRF4* reduced the high $^{15}NH_4^+$ uptake rate of NJ6-$GRF4^{ngr2}$, whereas transgenic expression of $GRF4^{ngr2}$ mRNA from its native promoter increased $^{15}NH_4^+$ uptake (Fig. 2c, Extended Data Fig. 1c).Overexpression of either $GRF4^{NGR2}$ or $GRF4^{ngr2}$ mRNA from the constitutive rice *Actin1* promoter conferred increased $^{15}NH_4^+$ uptake rates to NJ6 (Fig. 2c, Extended Data Fig. 1c). Thus, $GRF4^{ngr2}$ is equivalent to *qngr2*, confers an increased $^{15}NH_4^+$ uptake rate to NM73 and counteracts the repressive effects of *sd1*-mediated SLR1 accumulation.

[1]State Key Laboratory of Plant Cell and Chromosome Engineering, Institute of Genetics and Developmental Biology, Chinese Academy of Sciences, Beijing, China. [2]College of Life Sciences, University of Chinese Academy of Sciences, Beijing, China. [3]Hebei Laboratory of Crop Genetics and Breeding, Institute of Cereal and Oil Crops, Hebei Academy of Agriculture and Forestry Sciences, Shijiazhuang, China. [4]Department of Plant Sciences, University of Oxford, Oxford, UK. *e-mail: xdfu@genetics.ac.cn

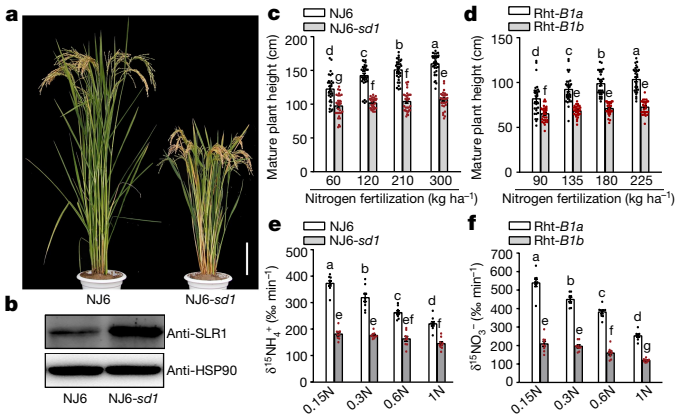

Fig. 1 | DELLA accumulation inhibits growth, nitrogen response and nitrogen uptake of rice and wheat GRVs. a, *Indica* rice variety NJ6 and near-isogenic NJ6-*sd1* plants. Scale bar, 15 cm. **b**, Accumulation of SLR1. Heat shock protein 90 (HSP90) serves as loading control. Blots are representative of three experiments performed independently with similar results. **c**, **d**, Heights of rice (**c**) and wheat (**d**) plants. Data are mean ± s.e.m. ($n = 30$). **e**, $^{15}NH_4^+$ uptake rates in varying nitrogen supply (0.15N, 0.1875 mM NH_4NO_3; 0.3N, 0.375 mM NH_4NO_3; 0.6N, 0.75 mM NH_4NO_3; 1N, 1.25 mM NH_4NO_3). **f**, $^{15}NO_3^-$ uptake rates in varying nitrogen supply (0.15N, 0.1875 mM $Ca(NO_3)_2$; 0.3N, 0.375 mM $Ca(NO_3)_2$; 0.6N, 0.75 mM $Ca(NO_3)_2$; 1N, 1.25 mM $Ca(NO_3)_2$). Data in **e**, **f** are mean ± s.e.m. ($n = 9$). **c**–**f**, Different letters denote significant differences ($P < 0.05$) from a Duncan's multiple range test.

GRF4^{NGR2} (NJ6) and *GRF4*^{ngr2} (NM73) allelic comparisons revealed multiple single nucleotide polymorphisms (SNPs) (Extended Data Fig. 1a, d), two of which (g.1187T>A and g.1188C>A in exon 3) prevent miR396-mediated cleavage of *GRF4*^{ngr2} mRNA[18–20], thus increasing *GRF4* mRNA and GRF4 abundance (Fig. 2d, Extended Data Fig. 1c) and promoting $^{15}NH_4^+$ uptake. Nevertheless, variety RD23, which lacks 1187A and 1188A, also displays a high $^{15}NH_4^+$ uptake rate (Fig. 2a, Extended Data Fig. 1d), and shares three *GRF4* promoter SNPs (g.−884T>A, g.−847C>T and g.−801C>T; Extended Data Fig. 1a, d) with NM73. In all, we detected three *GRF4* promoter haplotypes (A, as in 9311 and other *indica* varieties; B, with −884A, −847T and −801T, as in NM73 and RD23; and C, common in *japonica* germplasm; Extended Data Fig. 1d). Notably, *GRF4* mRNA abundance is higher in haplotype B-containing varieties TZZL1 and RD23 (Extended Data Fig. 1d) than in elite varieties carrying haplotypes A or C (Extended Data Fig. 1e, f), and presumably confers their relatively high $^{15}NH_4^+$ uptake rates (Fig. 2a). Thus, NM73 has the highest of all assayed $^{15}NH_4^+$ uptake rates because it combines the effects of promoter haplotype B with the miR396 resistance conferred by 1187A and 1188A[18–20].

We also found that in addition to regulating $^{15}NH_4^+$ uptake, *GRF4* is regulated by nitrogen supply. NJ6 *GRF4* mRNA abundance decreases with increasing nitrogen (Fig. 2e), probably owing to decreased *GRF4* transcription (miR396 abundance is not detectably increased with increasing nitrogen; Extended Data Fig. 1g), thus reducing GRF4 abundance (Fig. 2f). Because increased GRF4 abundance increases $^{15}NH_4^+$ uptake (Fig. 2c, d), our observations suggest that promotion of GRF4 abundance by low nitrogen enables feedback regulation of nitrogen homeostasis. In particular, the increased *GRF4* mRNA abundance response to low nitrogen is significantly amplified in varieties carrying haplotype B (for example, TZZL1 and RD23; Extended Data Fig. 1f). Finally, a CRISPR–Cas9[21]-generated semi-dwarf *grf4* mutant (Fig. 2g) lacks GRF4 (Fig. 2h, Extended Data Fig. 1a), and exhibits reduced $^{15}NH_4^+$ influx (Fig. 2i), reduced nitrogen-responsive regulation of $^{15}NH_4^+$ uptake (Fig. 2i) and reduced nitrogen-dependent biomass

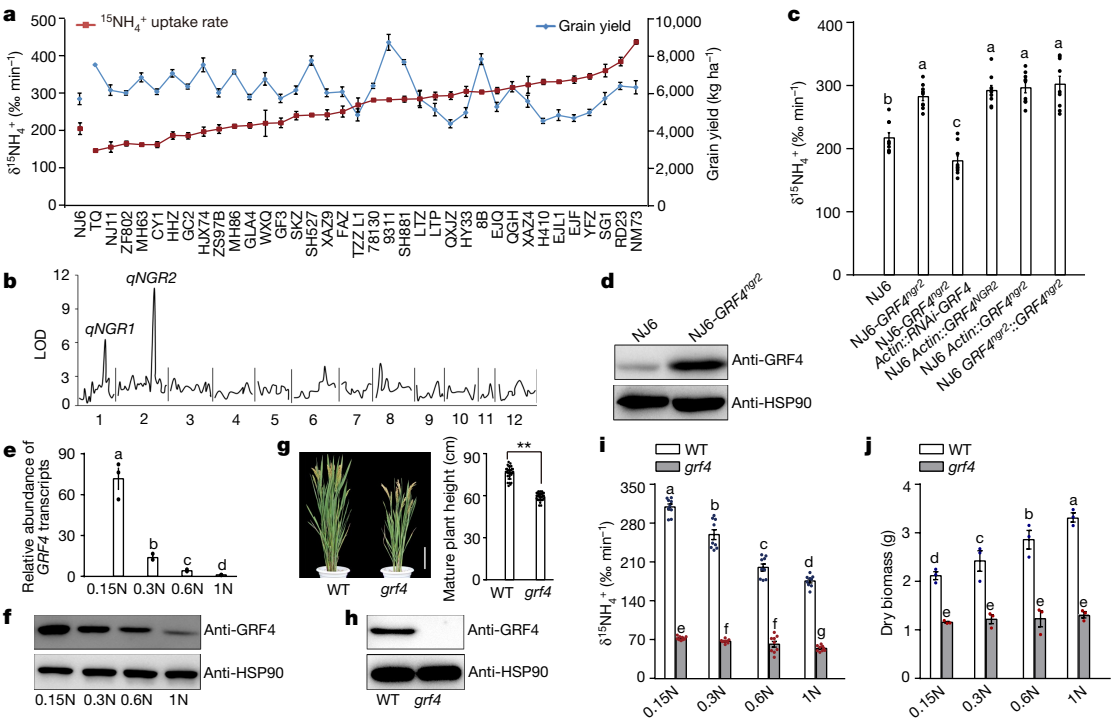

Fig. 2 | GRF4 regulates rice NH_4^+ uptake and growth response to nitrogen availability. a, Variation in $^{15}NH_4^+$ uptake and grain yield. Four-week-old rice plants ($^{15}NH_4^+$ uptake assays) were grown hydroponically with high nitrogen supply (1.25 mM NH_4NO_3). Field-grown rice plants (yield assays) were grown with urea supply (210 kg ha^{-1}). Data are mean ± s.e.m. of six plots (each plot contained 220 plants) per line. **b**, QTL analysis. **c**, $^{15}NH_4^+$ uptake rates. **d**, Accumulation of GRF4. **e**, *GRF4* transcript abundance in NJ6 roots grown in increasing nitrogen supply (0.15N, 0.1875 mM NH_4NO_3; 0.3N, 0.375 mM NH_4NO_3; 0.6N, 0.75 mM NH_4NO_3; 1N, 1.25 mM NH_4NO_3). Transcription is measured relative to 1N (set to one). **f**, Accumulation of GRF4 in NJ6. **g**, Mature plant height of the rice *grf4* mutant (Extended Data Fig. 1a). Scale bar, 15 cm. Data are mean ± s.e.m. ($n = 20$). **$P < 0.05$ compared to the wild-type (WT) group using a two-sided Student's *t*-test. **h**, Accumulation of GRF4. HSP90 serves as loading control (**d**, **f**, **h**). **i**, $^{15}NH_4^+$ uptake rate. Data in **c**, **i** are mean ± s.e.m. ($n = 9$). **j**, Dry weight of four-week-old plants. Data in **e**, **j** are mean ± s.e.m. ($n = 3$). **c**, **i**, **j**, Different letters denote significant differences ($P < 0.05$) from a Duncan's multiple range test. **b**, **d**, **f**, **h**, Data are representative of three experiments performed independently with similar results.

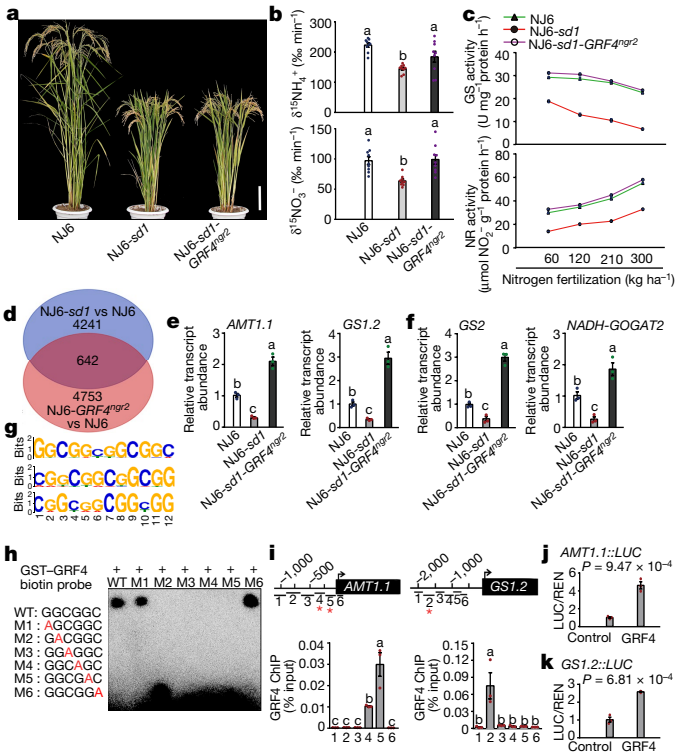

Fig. 3 | GRF4 regulates expression of multiple nitrogen-metabolism genes. a, Mature plants. Scale bar, 15 cm. **b**, $^{15}NH_4^+$ and $^{15}NO_3^-$ uptake rates. Data are mean ± s.e.m. ($n = 9$). **c**, Glutamine synthase (GS) and nitrate reductase (NR) activities in shoots of rice plants grown in paddy-field conditions with increasing urea supply. **d**, RNA-seq analysis: 4,883 genes were downregulated in NJ6-*sd1* (versus NJ6; blue), 5,395 genes were upregulated in NJ6-*GRF4*^{ngr2} (versus NJ6; orange) and 642 genes were common to both. **e**, **f**, Root (**e**) and shoot (**f**) mRNA abundances relative to NJ6 (set to one). **g**, Sequence motifs enriched in ChIP–seq with Flag-tagged GRF4. **h**, EMSA assays. Pictures in **a**, **h** are representative of three experiments performed independently with similar results. **i**, Flag–GRF4 mediated ChIP–PCR enrichment (relative to input) of GCGG-containing promoter fragments (marked with an asterisk) from *AMT1.1* and *GS1.2*. **b**, **e**, **f**, **i**, Different letters denote significant differences ($P < 0.05$) from a Duncan's multiple range test. **j**, **k**, Transactivation assays. **c**, **e**, **f**, **i**–**k**, Data are mean ± s.e.m. ($n = 3$). *P* values are from a two-sided Student's *t*-test.

accumulation (Fig. 2j). Thus, GRF4 is a nitrogen-responsive transcriptional regulator promoting both NH_4^+ uptake and growth in response to nitrogen supply, and counteracting the inhibitory effects of SLR1.

Regulation of nitrogen metabolism by GRF4–SLR1

We next determined how GRF4 and SLR1 counteract one another to regulate NH_4^+ assimilation. Although a NJ6-*sd1*-*GRF4*^{ngr2} isogenic line retains the semi-dwarfism, tiller numbers per plant and grain numbers per panicle conferred by *sd1* (Fig. 3a, Extended Data Fig. 2a–c), leaf and culm width and grain yield are increased (Extended Data Fig. 2d–f). In addition, the $^{15}NH_4^+$ uptake rate in NJ6-*sd1*-*GRF4*^{ngr2} is greater than in NJ6-*sd1* (and similar to that of NJ6) and $^{15}NO_3^-$ uptake is similarly affected (Fig. 3b). Furthermore, the activities of key nitrogen-assimilation enzymes, such as glutamine synthase (NH_4^+ assimilation)[22] and nitrate reductase (NO_3^- assimilation)[23] are, at varying nitrogen supply levels, consistently greater in NJ6-*sd1*-*GRF4*^{ngr2} than in NJ6-*sd1*, and similar to that of NJ6 (Fig. 3c). Thus, GRF4 promotes both nitrogen uptake and nitrogen assimilation, whereas SLR1 inhibits these processes.

Transcriptome-wide RNA sequencing (RNA-seq) analysis identified 642 genes with transcripts that were upregulated by GRF4 in NJ6-*GRF4*^{ngr2} and downregulated by SLR1 in NJ6-*sd1* (versus NJ6) (Fig. 3d, Supplementary Tables 2, 3). Among these, quantitative PCR with reverse transcription (RT–qPCR) confirmed root abundances of mRNAs encoding NH_4^+-uptake transporters (for example, *AMT1.1* and *AMT1.2*)[24] to be increased in NJ6-*sd1*-*GRF4*^{ngr2}, but reduced in NJ6-*sd1* (Fig. 3e, Extended Data Fig. 2g). Similarly, abundances of mRNAs encoding NH_4^+-assimilation enzymes (for example, *GS1.2*[23], *GS2* and *NADH-GOGAT2*) and corresponding enzymatic activities were relatively enhanced in NJ6-*sd1*-*GRF4*^{ngr2} (Fig. 3c, e, f, Extended Data Fig. 2h–j). Next, DNA sequencing of GRF4 chromatin-immunoprecipitation products (ChIP–seq) revealed potential GRF4 target-recognition sites, with a predominant GGCGGC motif being common to multiple nitrogen-metabolism gene promoters (Fig. 3g, Supplementary Table 4). Electrophoretic mobility shift assays (EMSA) demonstrated binding of glutathione *S*-transferase-tagged GRF4 to DNA fragments containing intact but not mutant GCGG core motifs (Fig. 3h), and ChIP–PCR confirmed in vivo association of GRF4 with GCGG-containing promoter fragments from multiple NH_4^+-metabolism genes, including *AMT1.1* and *GS1.2* (Fig. 3i, Extended Data Fig. 2k–n). Finally, GRF4 activates transcription from *AMT1.1* and *GS1.2* promoters in transactivation assays (Fig. 3j, k, Extended Data Fig. 2o). Further experiments demonstrated that GRF4-mediated transcriptional activation also promotes NO_3^- metabolism (Fig. 3b, c, Extended Data Fig. 3). Thus, GRF4 is a transcriptional activator of nitrogen metabolism, and counteracts the inhibitory effects of SLR1.

We next investigated how GA, SLR1 and GRF4 regulate nitrogen metabolism. GA promotes both $^{15}NH_4^+$ uptake rates to similarly high levels in NJ6 and NJ6-*sd1* (Fig. 4a). In addition, the GA-biosynthesis inhibitor pacolubutrazol[25] (PAC) reduces $^{15}NH_4^+$ uptake in NJ6 and NJ6-*sd1*, whereas GA restores it (Fig. 4a). Thus, SLR1 accumulation (owing to *sd1* or PAC) reduces NH_4^+ uptake, whereas SLR1 reduction (owing to GA) increases it. Furthermore, the GA–DELLA system differentially regulates the abundance of NH_4^+-metabolism mRNAs. *AMT1.1* and *GS1.2* mRNA abundances are increased by GA, reduced by PAC and restored by combined GA and PAC (Fig. 4b). We next found that PAC reduces ChIP–PCR enrichment of GCGG motif-containing fragments from the *AMT1.1* and *GS1.2* promoters, whereas GA promotes enrichment (Fig. 4c). Therefore, SLR1 accumulation inhibits binding of GRF4 to *AMT1.1* and *GS1.2* promoters (Fig. 4c), thus affecting mRNA abundance and NH_4^+ metabolism (Fig. 4a, b, Extended Data Fig. 4a, b), whereas SLR1 reduction promotes GRF4 binding. SLR1 abundance probably also affects NO_3^- uptake (Fig. 3b, Extended Data Fig. 3a, b) and nitrate reductase activity (Fig. 3c, Extended Data Fig. 4c) via inhibition of GRF4 activation of NO_3^--metabolism genes.

Although the interaction of GRF4 with GIF (GRF-interacting factor) co-activators via a conserved QLQ domain (Extended Data Fig. 5a, b) promotes expression of target genes[18], bimolecular fluorescence complementation (BiFC) and co-immunoprecipitation assays revealed that SLR1 interferes with this interaction (Fig. 4d–h, Extended Data Fig. 5c). In vivo fluorescence resonance energy transfer (FRET) assays demonstrated that SLR1 competitively inhibits the GRF4–GIF1 interaction, and that GA relieves this inhibition (Fig. 4f, g). Although the GRF4–GIF1 interaction promotes binding of GRF4 to GCGG motif-containing DNA fragments, SLR1 inhibits this promotion by inhibiting the GRF4–GIF1 interaction (but does not directly interfere with the DNA binding of GRF4; Fig. 4h). Accordingly, SLR1 inhibits GRF4–GIF1-mediated transactivation from *AMT1.1* and *GS1.2* promoters (Fig. 4i).

Notably, GRF4 abundance is self-promoted, and SLR1 inhibits that promotion. Although *GRF4* mRNA abundance is reduced in NJ6-*sd1* (versus NJ6) but increased in NJ6-*sd1*-*GRF4*^{ngr2} (versus NJ6-*sd1*; Extended Data Fig. 6a), GA increases *GRF4* mRNA abundance, and overcomes PAC-mediated reductions in *GRF4* mRNA abundance (Extended Data Fig. 6b). Furthermore, GRF4 binds in vivo with GCGG-containing *GRF4* promoter fragments (Extended Data Fig. 6c), and SLR1 inhibits GRF4–GIF1-mediated transcriptional activation of the *GRF4* promoter (Extended Data Fig. 6d). In consequence, SLR1 reduces GRF4 abundance by interfering with the GRF4–GIF1 interaction, whereas the *GRF4*^{ngr2} allele restores GRF4 abundance (Extended Data Fig. 6e; NJ6-*sd1* compared with NJ6-*sd1*-*GRF4*^{ngr2}). Thus, interference of SLR1 with the GRF4–GIF1 interaction counteracts the promotive effects of GRF4 on nitrogen metabolism in two ways.

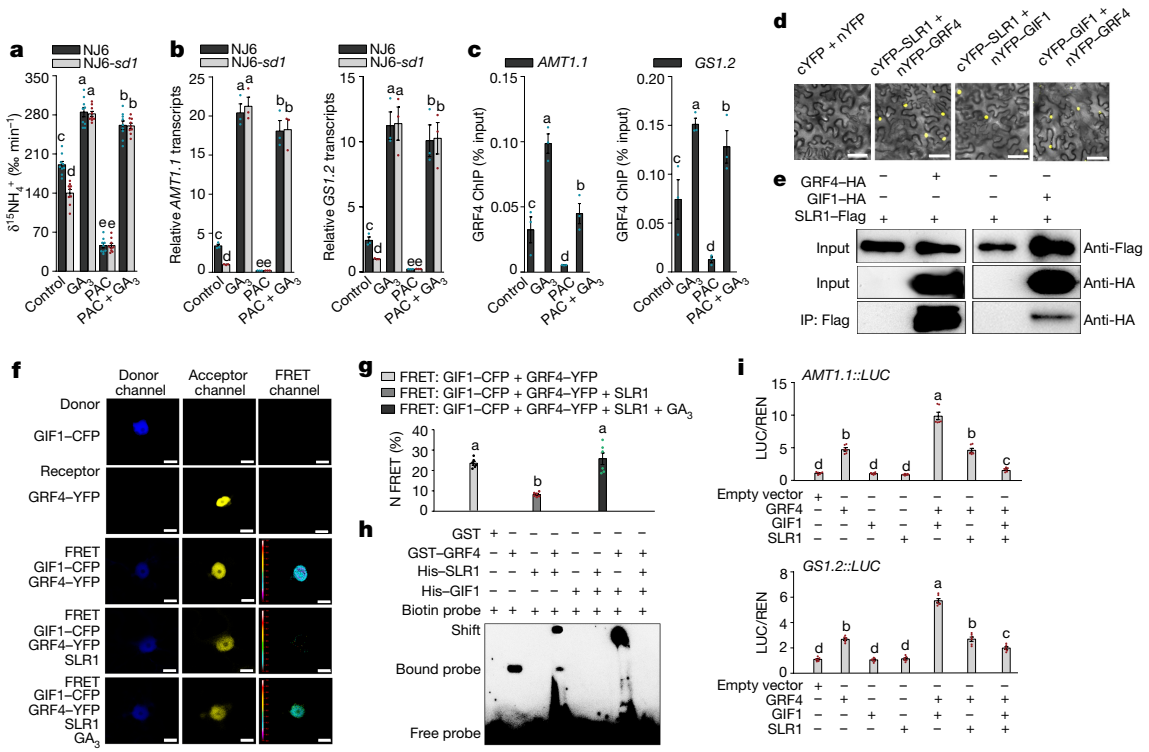

Fig. 4 | Competitive GRF4–GIF1–SLR1 interactions coordinate NH_4^+ uptake and assimilation. a, $^{15}NH_4^+$ uptake rates in four-week-old plants treated with 100 μM GA_3 and/or 2 μM paclobutrazol (PAC). Data are mean ± s.e.m. ($n = 9$). **b**, Root mRNA abundance relative to the level in NJ6-*sd1* plants (set to one). **c**, Extent of ChIP–PCR GRF4-mediated enrichment (relative to input) of GCGG-containing promoter fragments from *AMT1.1* (fragment 5) and *GS1.2* (fragment 2) (shown in Fig. 3i). Data in **b**, **c** are mean ± s.e.m. ($n = 3$). **d**, BiFC assays. Scale bar, 60 μm. cYFP, C-terminal portion of YFP; nYFP, N-terminal portion of YFP. When cYFP- and nYFP-tagged proteins are in close proximity, the cYFP and nYFP portions interact and produce YFP fluorescence. **e**, Co-immunoprecipitation experiments. HA, haemagglutinin. **f**, FRET images. Scale bar, 200 μm. **g**, Mean normalized FRET (N FRET) data for GIF1–CFP and GRF4–YFP channels. **h**, EMSA assays. GST, glutathione *S*-transferase. **d**–**f**, **h**, Pictures are representative of three experiments performed independently with similar results. **i**, Transactivation assays. The luciferase (LUC)/renilla (REN) activity obtained from co-transfection with an empty effector construct and indicated reporter constructs. The activity of the empty effector construct was set to one. **g**, **h**, Data are mean ± s.e.m. ($n = 6$). Different letters denote significant differences ($P < 0.05$) from Duncan's multiple range tests.

First, SLR1 reduces GRF4 accumulation. Second, SLR1 reduces GRF4–GIF1 activation of the transcription of nitrogen-metabolism genes.

GRF4–SLR1 links carbon fixation with growth

Although nitrogen metabolism is known to be coupled with the rate of photosynthetic carbon fixation[26], the molecular coupling mechanisms remain unknown. We next determined whether the GRF4–SLR1 interaction also regulates carbon assimilation. Transcriptome comparisons of NJ6, NJ6-*sd1* and NJ6-*sd1-GRF4*^{ngr2} (Fig. 3d, Supplementary Tables 2, 3) indicated that GRF4 upregulates multiple genes encoding regulatory components of photosynthesis (for example, *Lhca1* and *CAB1*), sucrose metabolism (for example, *TPS1* and *TPP1*) and sucrose transport (for example, *SWEET11* and *SWEET12*) (Extended Data Fig. 7a, b), whereas SLR1 downregulates these same genes. In addition, GRF4 binds in vivo to GCGG-containing promoter fragments from *PsbS1*, *TPS1* and *SWEET11* (Extended Data Fig. 7c), whereas SLR1 inhibits GRF4–GIF1 activation of transcription from *PsbS1*, *TPS1* and *SWEET11* promoters (Extended Data Fig. 7d). For selected photosynthetic genes (*Lhca1*, *Lhca3*, *Lhca4*, *Lhcb2*, *PsaD* and *PsaE*), we confirmed that encoded protein abundances in NJ6, NJ6-*sd1* and NJ6-*sd1-GRF4*^{ngr2} (Extended Data Fig. 7e) mirror the abundances of the respective encoding mRNAs (Extended Data Fig. 7a). Finally, we found that these effects on photosynthesis and carbon-assimilation gene expression affect carbon metabolism. First, in accordance with previous reports that semi-dwarfed GRVs have increased photosynthetic rates[27,28], we found the increased photosynthetic rate of NJ6-*sd1* (versus NJ6) to be still further increased in NJ6-*sd1-GRF4*^{ngr2} (Extended Data Fig. 7f). Furthermore, reductions in NJ6 biomass and carbon content conferred by *sd1* are reversed and further increased in NJ6-*sd1-GRF4*^{ngr2} (Extended Data Fig. 7g, h), but without affecting the carbon:nitrogen (C:N) ratio (Extended Data Fig. 7i). Thus, antagonistic GRF4–SLR1 interaction regulates and coordinates both nitrogen and carbon assimilation (hence maintaining the C:N ratio).

We also found that GRF4 upregulates multiple genes promoting cell division, including those encoding cyclin-dependent cdc2 protein kinases[29,30] (for example, *cycA1;1* and *cdc20 s-3*; Extended Data Fig. 7j), whereas SLR1 again downregulates these genes. This finding is consistent with the plant growth reduction in the *grf4* mutant (Fig. 2g). In addition, GRF4 binds in vivo to GCGG-containing promoter fragments from *cycA1;1* and *cdc20 s-3* (Extended Data Fig. 7k), and GA promotes GRF4–GIF1 activation of transcription from these same promoters (Extended Data Fig. 7l), whereas SLR1 inhibits activation by GRF4–GIF1. We conclude that GRF4–SLR1 antagonism modulates the GA-mediated promotion of cell proliferation, and integrates growth, nitrogen and carbon metabolism regulation.

GRF4 increases GRV NUE and grain yield

GRF4 promoter haplotype B (Extended Data Fig. 1d) exists in selected *indica* cultivars, but not in modern elite varieties. Nevertheless, among 225 accessions[31], haplotype B is associated with relatively high yield potential (Extended Data Fig. 8). We next showed that increasing GRF4 abundance improves NUE and grain yield of the high-yielding *sd1*-containing *indica* variety 9311. As for NJ6-*sd1-GRF4*^{ngr2} (Fig. 3a), the 9311-*GRF4*^{ngr2} isogenic line is not detectably changed with respect to the *sd1*-conferred semi-dwarf phenotype (Fig. 5a, b), but displays increased leaf and culm width (Extended Data Fig. 9a, b). However, the increased

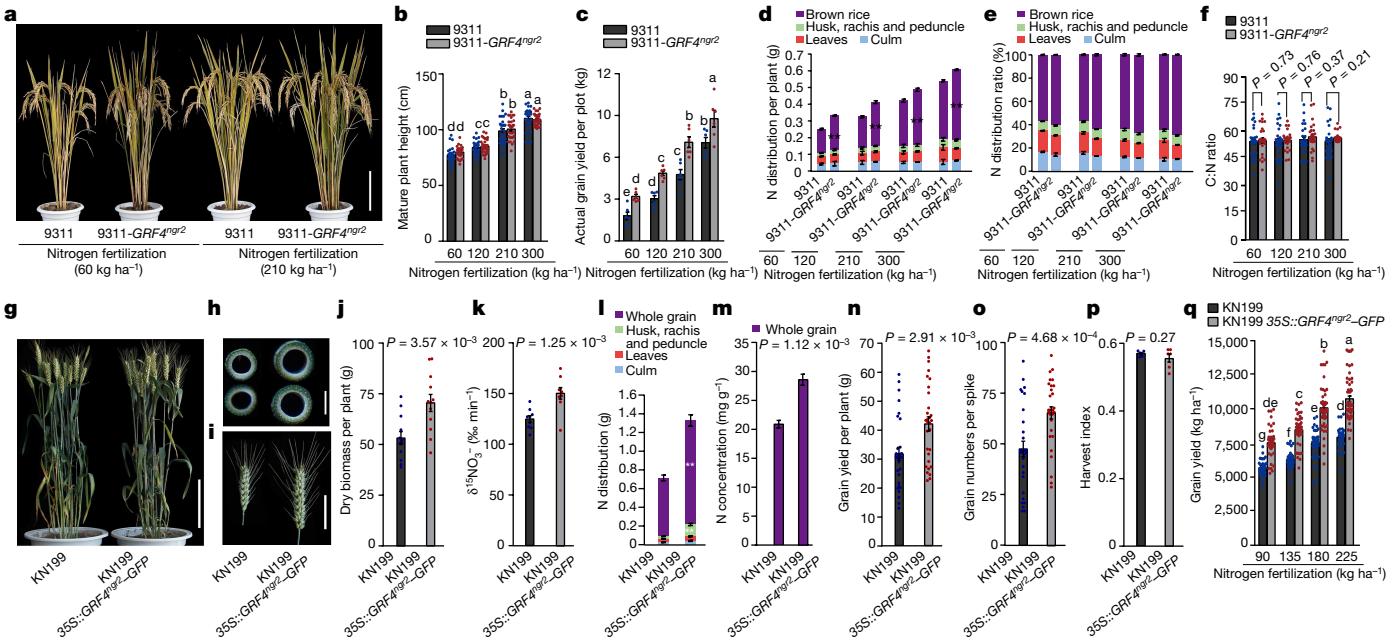

Fig. 5 | Increased GRF4 abundance boosts grain yield and NUE of rice and wheat GRVs without increasing mature plant height. a, Appearance of mature plants. Scale bar, 15 cm. **b**, Plant height. Data are mean ± s.e.m. ($n = 40$). **c**, Grain yield. Data are mean ± s.e.m. of six plots (each plot contained 220 plants) per line per nitrogen level. **d**, **e**, Absolute (**d**) and proportional (**e**) nitrogen distribution of plants shown in **b**. $^{**}P < 0.05$, 9311-*GRF4*^{ngr2} compared with 9311 by two-sided Student's *t*-test. **f**, C:N ratio of plants shown in **b**. Data in **d**–**f** are mean ± s.e.m. ($n = 30$). **g**, Mature wheat plant morphology. Scale bar, 15 cm. **h**, Cross-section of the uppermost internode of (left) KN199 and (right) KN199 *35S::GRF4*^{ngr2}*–GFP* wheat plants. Scale bar, 2 mm. **i**, Spike length. Scale bar, 5 cm. **a**, **g**–**i**, Pictures are representative of three experiments performed independently with similar results. **j**, Biomass accumulation. Data are mean ± s.e.m. ($n = 12$). **k**, $^{15}NO_3^-$ uptake rate. **l**, Nitrogen distribution. Data in **k**, **l** are mean ± s.e.m. ($n = 9$). $^{**}P < 0.05$, KN199 *35S::GRF4*^{ngr2}–GFP compared with KN199. **m**, Dry-weight nitrogen concentrations. Data are mean ± s.e.m. ($n = 20$). **n**, Grain yield. **o**, Grain number. Data in **n**, **o** are mean ± s.e.m. ($n = 30$). **p**, Harvest index. Data are mean ± s.e.m. ($n = 6$). **q**, Overall grain yield. Data are mean ± s.e.m. ($n = 60$). **f**, **j**, **k**, **m**–**p**, *P* values are from two-sided Student's *t*-tests. **b**, **c**, **q**, Different letters denote significant differences ($P < 0.05$) from a Duncan's multiple range test.

$^{15}NH_4^+$ and $^{15}NO_3^-$ uptake conferred by *GRF4*^{ngr2} (Extended Data Fig. 9c, d) enhances 9311 grain yield and NUE. Grain yield per plot was increased in 9311-*GRF4*^{ngr2} (versus 9311) at both high and low levels of nitrogen supply (Fig. 5c), owing to increases in both grain number and grain weight[18–20] (Extended Data Fig. 9e, f). Harvest index was relatively unaffected (Extended Data Fig. 9g), presumably because biomass increases (Extended Data Fig. 9h) balance out increases in grain yield (Fig. 5c). Although total nitrogen in above-ground parts of 9311-*GRF4*^{ngr2} was greater than in 9311 (Fig. 5d), the distribution ratio of nitrogen allocated to grain (versus vegetative organs) was not significantly increased (Fig. 5e) and the C:N ratio was not detectably affected (Fig. 5f). Thus, the increased GRF4 abundance conferred by *GRF4*^{ngr2} partially disconnects GA regulation of stem elongation (plant height) from nitrogen metabolic regulation. GRF4-promoted biomass increases are reflected primarily in increased leaf and culm widths rather than height.

Chinese *japonica* rice GRV semi-dwarfism is conferred by a mutant variant (dep1-1) of the Gγ subunit[32] that reduces vegetative growth nitrogen response and increases NUE[22]. We found that increasing GRF4 abundance (GRF4–GFP in transgenic WYJ7-*dep1-1*[22] plants expressing *35S::GRF4*^{ngr2}*-GFP*) did not suppress *dep1-1*-conferred semi-dwarfism (Extended Data Fig. 10a), but increased both $^{15}NH_4^+$ and $^{15}NO_3^-$ uptake rates (Extended Data Fig. 10b–d). In addition, although plant height, heading date and tiller numbers per plant in response to different nitrogen supply rates were unaffected (Extended Data Fig. 10e–g), overexpression of *GRF4*^{ngr2}*–GFP* increased both grain number (in low nitrogen; Extended Data Fig. 10h) and grain yield (Extended Data Fig. 10i) of WYJ7-*dep1-1*. Nutrient assimilation and grain yield of rice GRVs can thus be increased by higher GRF4 abundance, particularly at low nitrogen fertilization levels, without simultaneously causing yield-reducing plant height increases.

Finally, the semi-dwarfism of high-yielding Chinese wheat GRV KN199 is conferred by the mutant *Rht-B1b* allele[5,6]. As in rice, transgenic expression of *35S::GRF4*^{ngr2}*–GFP* did not increase KN199 plant height (Fig. 5g), but did increase culm diameter and wall thickness (Fig. 5h), spike length (Fig. 5i) and biomass accumulation (Fig. 5j). In addition, *35S::GRF4*^{ngr2}*–GFP* increased the $^{15}NO_3^-$-uptake rate of KN199 (Fig. 5k), total nitrogen in above-ground plant parts (Fig. 5l) and nitrogen concentration in de-husked grain (Fig. 5m). *35S::GRF4*^{ngr2}*–GFP* also boosted KN199 yield (Fig. 5n) by increasing grain numbers per spike (Fig. 5o), without affecting harvest index (Fig. 5p). Moreover, the improvement of grain yield conferred on KN199 by *35S::GRF4*^{ngr2}*–GFP* at low nitrogen supply shows that increased GRF4 abundance enhances both grain yield and NUE of wheat GRVs (Fig. 5q), without affecting the beneficial GRV semi-dwarfism. Indeed, the increased culm width and wall thickness conferred by *35S::GRF4*^{ngr2}*–GFP* (Fig. 5h) is likely to enhance the stem robustness conferred by mutant *Rht* alleles, thus further reducing lodging yield loss. In conclusion, increased GRF4 abundance increases grain yields of rice and wheat GRVs grown in moderate nitrogen conditions.

Discussion

We here report new advances in fundamental plant science and strategic plant breeding. First, the GRF4–DELLA interaction integrates plant growth and metabolic regulation. GRF4 is a transcriptional regulator of multiple nitrogen-metabolism genes that, because it is itself nitrogen regulated, probably confers homeostatic coordination of plant nitrogen metabolism. Notably, nitrogen-regulated GRF4 also coordinates carbon metabolism and growth, and is thus likely to confer broader-range integrative homeostatic control. Although long thought to exist, the identities of such broad-range growth and metabolic integrators were previously unknown. Furthermore, GRF4 activity is balanced by an antagonistic regulatory relationship with the DELLA growth repressor. Essentially, physical DELLA–GRF4–GIF1 interactions enable DELLA to inhibit activation of target gene promoters by GRF4–GIF1, and the balance between opposing GRF4 and DELLA activities thus enhances coordinated regulation of plant growth and metabolism.

Second, increasing the abundance of GRF4 in GRVs tips the GRF4–DELLA balance to favour GRF4, conferring increases in carbon and nitrogen assimilation, biomass, leaf and stem width, but having little effect on plant height[33]. The practical plant breeding consequence of this is that it enables enhanced GRV nutrient assimilation without the loss of the beneficial semi-dwarfism conferred by DELLA accumulation. GRV NUE can thus be improved, without the yield penalties of increased lodging. Genetic variation of *GRF4* (and orthologues) should now become a major target for breeders in enhancing crop yield and nutrient-use efficiency. Such enhancements will enable future green revolutions, sustainably increasing yield, yet reducing environmentally degrading agricultural nitrogen use.

Online content

Any Methods, including any statements of data availability and Nature Research reporting summaries, along with any additional references and Source Data files, are available in the online version of the paper at https://doi.org/10.1038/s41586-018-0415-5.

Received: 9 February 2018; Accepted: 5 July 2018;
Published online 15 August 2018.

1. Khush, G. S. Green revolution: preparing for the 21st century. *Genome* **42**, 646–655 (1999).
2. Pingali, P. L. Green revolution: impacts, limits, and the path ahead. *Proc. Natl Acad. Sci. USA* **109**, 12302–12308 (2012).
3. Evenson, R. E. & Gollin, D. Assessing the impact of the green revolution, 1960 to 2000. *Science* **300**, 758–762 (2003).
4. Hedden, P. The genes of the green revolution. *Trends Genet.* **19**, 5–9 (2003).
5. Peng, J. et al. 'Green revolution' genes encode mutant gibberellin response modulators. *Nature* **400**, 256–261 (1999).
6. Zhang, C., Gao, L., Sun, J., Jia, J. & Ren, Z. Haplotype variation of green revolution gene *Rht-D1* during wheat domestication and improvement. *J. Integr. Plant Biol.* **56**, 774–780 (2014).
7. Sasaki, A. et al. Green revolution: a mutant gibberellin-synthesis gene in rice. *Nature* **416**, 701–702 (2002).
8. Spielmeyer, W., Ellis, M. H. & Chandler, P. M. Semidwarf (*sd-1*), "green revolution" rice, contains a defective gibberellin 20-oxidase gene. *Proc. Natl Acad. Sci. USA* **99**, 9043–9048 (2002).
9. Harberd, N. P., Belfield, E. & Yasumura, Y. The angiosperm gibberellin–GID1–DELLA growth regulatory mechanism: how an "inhibitor of an inhibitor" enables flexible response to fluctuating environments. *Plant Cell* **21**, 1328–1339 (2009).
10. Xu, H., Liu, Q., Yao, T. & Fu, X. Shedding light on integrative GA signaling. *Curr. Opin. Plant Biol.* **21**, 89–95 (2014).
11. Itoh, H., Ueguchi-Tanaka, M., Sato, Y., Ashikari, M. & Matsuoka, M. The gibberellin signaling pathway is regulated by the appearance and disappearance of SLENDER RICE1 in nuclei. *Plant Cell* **14**, 57–70 (2002).
12. Asano, K. et al. Artificial selection for a green revolution gene during *japonica* rice domestication. *Proc. Natl Acad. Sci. USA* **108**, 11034–11039 (2011).
13. Gooding, M. J., Addisu, M., Uppal, R. K., Snape, J. W. & Jones, H. E. Effect of wheat dwarfing genes on nitrogen-use efficiency. *J. Agric. Sci.* **150**, 3–22 (2012).
14. Li, B.-Z. et al. Molecular basis and regulation of ammonium transporter in rice. *Rice Sci.* **16**, 314–322 (2009).
15. Hawkesford, M. J. Reducing the reliance on nitrogen fertilizer for wheat production. *J. Cereal Sci.* **59**, 276–283 (2014).
16. Zhao, X. et al. Nitrogen runoff dominates water nitrogen pollution from rice-wheat rotation in the Taihu Lake region of China. *Agric. Ecosyst. Environ.* **156**, 1–11 (2012).
17. Conway, G. *One Billion Hungry. Can We Feed the World?* (Cornell Univ. Press, Ithaca, 2012).
18. Che, R. et al. Control of grain size and rice yield by *GL2*-mediated brassinosteroid responses. *Nat. Plants* **2**, 15195 (2015).
19. Duan, P. et al. Regulation of Os*GRF4* by *Os*miR396 controls grain size and yield in rice. *Nat. Plants* **2**, 15203 (2015).
20. Hu, J. et al. A rare allele of *GS2* enhances grain size and grain yield in rice. *Mol. Plant* **8**, 1455–1465 (2015).
21. Ma, X. et al. A robust CRISPR/Cas9 system for convenient, high-efficiency multiplex genome editing in monocot and dicot plants. *Mol. Plant* **8**, 1274–1284 (2015).
22. Sun, H. et al. Heterotrimeric G proteins regulate nitrogen-use efficiency in rice. *Nat. Genet.* **46**, 652–656 (2014).
23. Somers, D. A., Kuo, T. M., Kleinhofs, A., Warner, R. L. & Oaks, A. Synthesis and degradation of barley nitrate reductase. *Plant Physiol.* **72**, 949–952 (1983).
24. Tabuchi, M., Abiko, T. & Yamaya, T. Assimilation of ammonium ions and reutilization of nitrogen in rice (*Oryza sativa* L.). *J. Exp. Bot.* **58**, 2319–2327 (2007).
25. Peng, J. et al. The *Arabidopsis GAI* gene defines a signaling pathway that negatively regulates gibberellin responses. *Genes Dev.* **11**, 3194–3205 (1997).
26. Nunes-Nesi, A., Fernie, A. R. & Stitt, M. Metabolic and signaling aspects underpinning the regulation of plant carbon nitrogen interactions. *Mol. Plant* **3**, 973–996 (2010).
27. LeCain, D. R., Morgan, J. A. & Zerbi, G. Leaf anatomy and gas exchange in nearly isogenic semidwarf and tall winter wheat. *Crop Sci.* **29**, 1246–1251 (1989).
28. Morgan, J. A., LeCain, D. R. & Wells, R. Semidwarfing genes concentrate photosynthetic machinery and affect leaf gas exchange of wheat. *Crop Sci.* **30**, 602–608 (1990).
29. Fabian, T., Lorbiecke, R., Umeda, M. & Sauter, M. The cell cycle genes *cycA1;1* and *cdc2Os-3* are coordinately regulated by gibberellin in planta. *Planta* **211**, 376–383 (2000).
30. Sauter, M. Differential expression of a CAK (cdc2-activating kinase)-like protein kinase, cyclins and *cdc2* genes from rice during the cell cycle and in response to gibberellin. *Plant J.* **11**, 181–190 (1997).
31. Yu, J. et al. *OsLG3* contributing to rice grain length and yield was mined by Ho-LAMap. *BMC Biol.* **15**, 28 (2017).
32. Huang, X. et al. Natural variation at the *DEP1* locus enhances grain yield in rice. *Nat. Genet.* **41**, 494–497 (2009).
33. Serrano-Mislata, A. et al. *DELLA* genes restrict inflorescence meristem function independently of plant height. *Nat. Plants* **3**, 749–754 (2017).

Acknowledgements We thank J. F. Ma for comments on this manuscript. This research was supported by grants from the National Key Research and Development Program of China (2016YFD0100401, 2016YFD0100706 and 2016YFD0100901), National Natural Science Foundation of China (91635302), Chinese Academy of Sciences (XDA08010101) and by the Biological and Biotechnological Sciences Research Council (UK) 'Newton Fund' Rice Research Initiative grant BB/M011224/1.

Reviewer information *Nature* thanks B. Hirel, M. Matsuoka and the other anonymous reviewer(s) for their contribution to the peer review of this work.

Author contributions S.L. performed most of the experiments; Y.Ti. and S.L. conducted QTL analysis; S.L., J.Z. and K.W. constructed near isogenic lines; S.L., Y.Y. and Q.L. performed field experiments; Y.To., M.H. and H.L. characterized the phenotypes of transgenic wheat plants; J.Y. performed haplotype analysis; N.P.H. and X.F. designed experiments; N.P.H. and X.F. wrote the manuscript. All authors discussed the results and contributed to the manuscript.

Competing interests The authors declare no competing interests.

Additional information
Extended data is available for this paper at https://doi.org/10.1038/s41586-018-0415-5.
Supplementary information is available for this paper at https://doi.org/10.1038/s41586-018-0415-5.
Reprints and permissions information is available at http://www.nature.com/reprints.
Correspondence and requests for materials should be addressed to X.F.
Publisher's note: Springer Nature remains neutral with regard to jurisdictional claims in published maps and institutional affiliations.

METHODS

Plant materials and field growth conditions. Details of rice germplasm used for positional cloning and haplotype analysis have been described elsewhere[22,31,34]. QTL analysis and map-based cloning were performed using BC_1F_2, BC_2F_2 and BC_3F_2 populations derived from a cross between selected variety NM73 and *indica* variety NJ6 (the recurrent parent). Near isogenic line (NIL) plants carrying differing combinations of the *qngr2* and *sd1* alleles were bred by crossing NM73 × NJ6 and NM73 × 9311 F_1 six times with NJ6, NJ6-*sd1* and 9311 as recurrent parents. Field-grown NILs and transgenic rice plants were raised in standard paddy conditions with an interplant spacing of 20 cm at the Institute of Genetics and Developmental Biology experimental station sites located in Lingshui (Hainan Province), Hefei (Anhui Province) and Beijing as previously described[22,32]. Field-grown wheat plants (Chinese wheat GRV KN199 and transgenic derivatives) were planted during the winter planting season at the Experimental Station of the Institute of Cereal and Oil Crops, Hebei Academy of Agriculture and Forestry Sciences (Shijiazhuang, Hebei province).

Hydroponic culture conditions. Hydroponic culture conditions were modified from previously published work[35]. Seeds were disinfected in 20% sodium hypochlorite solution for 30 min, thoroughly washed with deionized water, and then germinated in moist Perlite. Seven-day-old seedlings were then selected and transplanted to PVC pots containing 40 l + nitrogen nutrient solution (1.25 mM NH_4NO_3, 0.5 mM $NaH_2PO_4{\cdot}2H_2O$, 0.75 mM K_2SO_4, 1 mM $CaCl_2$, 1.667 mM $MgSO_4{\cdot}7H_2O$, 40 μM Fe–EDTA (Na), 19 μM H_3BO_3, 9.1 μM $MnSO4{\cdot}H_2O$, 0.15 μM $ZnSO_4{\cdot}7H_2O$, 0.16 μM $CuSO_4$ and 0.52 μM $(NH_4)_3Mo_7O_{24}{\cdot}4H_2O$, pH 5.5). The compositions of nutrient solutions containing different levels of supplied nitrogen were as follows: 1N, 1.25 mM NH_4NO_3; 0.6N, 0.75 mM NH_4NO_3; 0.3N, 0.375 mM NH_4NO_3; 0.15N, 0.1875 mM NH_4NO_3. All nutrient solutions were changed twice per week, pH was adjusted to 5.5 every day. The temperature was maintained at 30 °C day and 22 °C night, and the relative humidity was 70%.

Positional cloning of *qNGR2*. The map-based cloning of *qngr2* was based on 1,849 BC_2F_2 and 3,124 BC_3F_2 populations derived from the backcross between the selected variety NM73 and the *indica* rice variety NJ6 (with NJ6 as the recurrent parent). Primer sequences used for map-based cloning and genotyping assays are given in Supplementary Table 5.

Transgene constructs. The $GRF4^{NGR2}$ mRNA-encoding sequence (together with intron sequences) was amplified from NJ6. The $GRF4^{ngr2}$ mRNA-coding sequence (together with introns and/or promoter regions lying approximately 3-kb upstream of the transcription start site) was amplified from NM73. These amplified genomic DNA fragments were then inserted into the *Actin::nos*[36] and *CAMBIA2300* (CAMBIA, http://www.cambia.org/) vectors to respectively generate the *Actin::*$GRF4^{NGR2}$ and $GRF4^{ngr2}$*::*$GRF4^{ngr2}$ constructs. A full-length $GRF4^{ngr2}$ cDNA was introduced into the *35S::GFP-nos*[22] and *35S::Flag-nos*[34] vectors to generate the *35S::*$GRF4^{ngr2}$*–GFP* and *35S::Flag–*$GRF4^{ngr2}$ constructs. A 300-bp $GRF4^{ngr2}$ cDNA fragment was amplified and used to construct the *Actin::RNAi-GRF4* transgene, as described elsewhere[32]. gRNA constructs required for construction of the CRISPR–Cas9-generated *GRF4* loss of function allele (*grf4*) in the WYJ7 genetic background were made as described elsewhere[21,34]. Transgenic rice and wheat plants were generated by *Agrobacterium*-mediated transformation as described elsewhere[32]. Relevant primer sequences are given in Supplementary Table 6.

RT–qPCR. Total RNAs were extracted from different organs of three-week-old rice plants under hydroponic conditions using the TRIzol reagent (Invitrogen), and then treated with RNase-free DNase I (Invitrogen) according to the manufacturer's protocol. Full-length cDNA was then reverse transcribed using a cDNA synthesis kit (TRANSGEN, AE311). qPCR was performed according to the manufacturer's instructions (TRANSGEN, AQ101), using three independent RNA preparations as biological replicates. Rice *Actin2* gene transcripts were used as a reference. The relevant primer sequences are given in Supplementary Table 7.

Bimolecular fluorescence complementation (BiFC) assays. The full-length cDNAs corresponding to the *SLR1*, *GIF1*, *GIF2*, *GIF3*, *GRF1*, *GRF2*, *GRF3*, *GRF4*, *GRF5*, *GRF6*, *GFR7*, *GRF8*, *GRF9*, *GRF10*, *GRF11* and *GRF12* genes, along with both deleted and non-deleted versions of *GRF4* cDNA were amplified from NJ6. The resultant amplicons were inserted into the *pSY-735-35S-cYFP-HA* or *pSY-736-35S-nYFP-EE* vectors[37] to generate fusion constructs. Co-transfection of constructs (for example, those encoding nYFP–GRF4 and cYFP–SLR1) into tobacco leaf epidermal cells by *Agrobacterium*-mediated infiltration enabled testing for protein–protein interactions. After 48 h incubation in the dark, the YFP signal was examined and photographed using a confocal microscope (Zeiss LSM710). Each BiFC assay was repeated at least three times. Relevant primer sequences are given in Supplementary Table 6.

Co-immunoprecipitation and western blotting. Full-length *GRF4*, *GIF1* and *SLR1* cDNAs were amplified, and then inserted into either the *pUC-35S-HA-RBS* or the *pUC-35S-Flag-RBS* vector as previously described[38]. *A. thaliana* protoplasts were transfected with 100 μg of plasmid and then incubated overnight in low light intensity conditions. Total protein was then extracted from harvested protoplasts by treating with 50 mM HEPES (pH 7.5), 150 mM KCl, 1 mM EDTA (pH8), 0.3% Triton X-100, 1 mM DTT with added proteinase inhibitor cocktail (Roche LifeScience). Lysates were incubated with magnetic beads conjugated with an anti-DDDDK-tag antibody (MBL, M185-11) at 4 °C for at least 4 h. The magnetic beads were then rinsed six times with the extraction buffer and eluted with 3 × Flag peptide (Sigma-Aldrich, F4709). Immunoprecipitates were electrophoretically separated by SDS–PAGE and transferred to a nitrocellulose membrane (GE Healthcare). Proteins were detected by immunoblot using the antibodies anti-Flag (Sigma, F1804) and anti-HA (MBL, M180-7). In addition, the GRF4, SLR1, Lhca1, Lhca3, Lhca4, Lhcb2, PsaD and PsaE proteins were detected by probing the membrane with anti-GRF4 antibodies (Abmart), anti-SLR1 antibodies (ABclonal Technology), anti-Lhca1 antibodies (Agrisera, AS01005), anti-Lhca3 antibodies (Agrisera, AS01007), anti-Lhca4 antibodies (Agrisera, AS01008), anti-Lhcb2 antibodies (Agrisera, AS01003), anti-PsaD antibodies (Agrisera, AS09461) and anti-PsaE antibodies (Agrisera, AS08324A), respectively. Uncropped blots are shown in Supplementary Fig. 1. Relevant primer sequences are given in Supplementary Table 6.

EMSA assays. EMSA was performed as previously described with minor modifications[39]. Full-length *GIF1* and *SLR1* cDNAs were amplified and cloned into the *pCold-TF* vector (Takara). His–GIF1 and His–SLR1 recombinant proteins were purified using Ni–NTA agarose (QIAGEN, 30210), following the manufacturer's instructions. GST and GST–GRF4 recombinant proteins were expressed in the *Escherichia coli* BL21 (DE3) strain and then purified using Glutathione Sepharose 4B beads (GE Healthcare, 17-0756-01). DNA probes (42 bp) were artificially amplified and labelled using a biotin label kit (Biosune). DNA gel shift assays were performed using the LightShift Chemiluminescent EMSA kit (Thermo Fisher Scientific, 20148). Relevant primer sequences are given in Supplementary Table 8.

RNA-seq analysis. Total RNAs were extracted from three-week-old rice plants grown under high nitrogen conditions (1.25 mM NH_4NO_3) using the QIAGEN RNeasy plant mini kit (QIAGEN, 74904) following the manufacturer's instructions. Three replicate RNA-seq libraries were prepared from NJ6, NJ6-*sd1* and NJ6-$GRF4^{ngr2}$ plants. A total of the nine libraries were sequenced separately using the BGISEQ-500 sequencer. For each RNA sample, the NIL plants were collected from three replicates and pooled together after RNA extraction. Raw sequencing reads were cleaned by removing adaptor sequences, reads containing poly-N sequences, and low-quality reads. Approximately 24,006,405 clean reads were mapped to the Nipponbare reference genome using HISAT[40]/Bowtie2[41] tools. After data were mapped, normalization was performed and then FPKM (fragments per kilobase per million mapped reads) was calculated using RESM software[42]. As previously described[43], a false discovery rate (FDR) < 0.01 and absolute value of $\log_2$ ratio ≥ 2 were used to identify differentially expressed genes in NJ6-*sd1* versus NJ6 and NJ6-$GRF4^{ngr2}$ versus NJ6 samples. Comparisons of the three individual replicate FPKM values of the genes involved in the coordinated regulation of plant growth and nitrogen, and carbon metabolism are given in Supplementary Table 3.

ChIP–seq and ChIP–qPCR assays. ChIP assays were performed as previously described with minor modifications[44]. Approximately 2 g of two-week-old seedlings of transgenic *35S::Flag–*$GRF4^{ngr2}$ rice plants grown under the high nitrogen (1.25 mM NH_4NO_3) conditions were fixed with 1% (v/v) formaldehyde under vacuum for 15 min at 20–25 °C, and then homogenized in liquid nitrogen. After isolation and lysing of nuclei, the chromatin complexes were isolated and ultrasonically fragmented into fragments with an average size of approximately 500 bp. Immunoprecipitations were performed with anti-Flag antibodies (Sigma, F1804) overnight at 4 °C. The precipitated DNA was recovered and dissolved in water and stored at −80 °C. Illumina sequencing libraries were constructed according to the manufacturer's instructions, and then sequenced on the BGISEQ-500 platform. Sequencing reads were mapped to the Nipponbare reference genome using SOAP aligner/soap2[45]. The peak summits were used to define the peak location types on the genome, and motif search and classification were performed as previously described[46]. In addition, the precipitated DNA samples served as template for RT–qPCR. Relevant primer sequences are given in Supplementary Table 9.

FRET assay. Cauliflower mosaic virus 35S promoter-driven fusion constructs with C-terminal tagging of CFP or YFP were created to generate the donor vector *35S::GIF1–CFP* and the acceptor vector *35S::GRF4–YFP*. Donor and acceptor vectors, with or without a *35S::SLR1* vector and/or GA (GA_3), were co-transformed into tobacco leaf epidermis cells by *Agrobacterium*-mediated infiltration to provide the FRET signal. Transformation with *35S::GIF1–CFP* vector only provided the donor signal, and transformation with *35S::GRF4–YFP* vector only provided the acceptor signal. The FRET signal was detected and photographed using a confocal microscope (Zeiss LSM710). Relevant primer sequences are given in Supplementary Table 6.

In vitro transient transactivation assays. Approximately 2-kb DNA promoter fragments from each of *AMT1.1*, *AMT1.2*, *NRT1.1B*, *NRT2.3a*, *NPF2.4*, *GS1.2*, *GS2*, *NADH-GOGAT2*, *Fd-GOGAT*, *NIA1*, *NIA3*, *NiR1*, *PsbS1*, *TPS1*, *SWEET11*, *cycA1;1*, *cdc2-3*, or *GRF4* were amplified from NJ6, and then subcloned into a *pUC19* vector

containing the firefly luciferase reporter gene driven by the 35S minimal TATA box and 5 × GAL4 binding elements, thus generating reporter plasmids containing specific promoters fused to luciferase. The full-length *GRF4* cDNA was amplified and fused to sequence encoding GAL4BD, thus generating the effector plasmid *RTBD-GRF4*. Transient transactivation assays were performed using rice protoplasts as described elsewhere[47]. The Dual-Luciferase Reporter Assay System (Promega, E1960) was used to perform the luciferase activity assay, with the Renilla luciferase gene as an internal control. Relevant primer sequences are given in Supplementary Table 6.

Determination of plant carbon and nitrogen concentrations. Samples from various plant organs were dried in an oven at 80 °C for 72 h. After tissue homogenization, carbon and nitrogen concentrations were determined using an elemental analyser (IsoPrime100; Elementar). All experiments were conducted with at least three replicates.

^{15}N uptake analysis. After growth in hydroponic culture for 4 weeks, rice root $^{15}NO_3^-$ and $^{15}NH_4^+$ influx measurements were as described elesewhere[48,49]. Roots and shoots were separated and stored at −70 °C before freeze drying. Roots and shoots were dried overnight at 80 °C, and the ^{15}N content was measured using the Isoprime 100 (Elementar, Germany).

Determination of glutamine synthase and nitrate reductase activities. Glutamine synthase and nitrate reductase activities were determined with the Glutamine Synthetase Kit (Solarbio LIFE SCIENCES, BC0910) and the Nitrate Reductase Kit (Solarbio LIFE SCIENCES, BC0080) following the manufacturer's instructions.

Reporting summary. Further information on experimental design is available in the Nature Research Reporting Summary linked to this paper.

Data availability. Sequencing data that support the findings of this study have been deposited in the Gene Expression Omnibus (GEO) with the accession code GSE114287. Source Data (including uncropped western blots and RNA-seq data) generated and/or analysed in the current study and Supplementary Information are provided with the online version of the paper. All other data are available from the corresponding author upon reasonable request.

34. Wang, S. et al. Non-canonical regulation of SPL transcription factors by a human OTUB1-like deubiquitinase defines a new plant type rice associated with higher grain yield. *Cell Res.* **27**, 1142–1156 (2017).
35. Liu, W.-J., Zhu, Y.-G., Smith, F. A. & Smith, S. E. Do phosphorus nutrition and iron plaque alter arsenate (As) uptake by rice seedlings in hydroponic culture? *New Phytol.* **162**, 481–488 (2004).
36. Wang, S. et al. Control of grain size, shape and quality by Os*SPL16* in rice. *Nat. Genet.* **44**, 950–954 (2012).
37. Bracha-Drori, K. et al. Detection of protein–protein interactions in plants using bimolecular fluorescence complementation. *Plant J.* **40**, 419–427 (2004).
38. Chen, H. et al. Firefly luciferase complementation imaging assay for protein–protein interactions in plants. *Plant Physiol.* **146**, 368–376 (2008).
39. Chen, L. et al. *Os*MADS57 together with *Os*TB1 coordinates transcription of its target Os*WRKY94* and *D14* to switch its organogenesis to defense for cold adaptation in rice. *New Phytol.* **218**, 219–231 (2018).
40. Kim, D., Langmead, B. & Salzberg, S. L. HISAT: a fast spliced aligner with low memory requirements. *Nat. Methods* **12**, 357–360 (2015).
41. Langmead, B., Trapnell, C., Pop, M. & Salzberg, S. L. Ultrafast and memory-efficient alignment of short DNA sequences to the human genome. *Genome Biol.* **10**, R25 (2009).
42. Li, B. & Dewey, C. N. RSEM: accurate transcript quantification from RNA-seq data with or without a reference genome. *BMC Bioinformatics* **12**, 323 (2011).
43. Benjamini, Y., Drai, D., Elmer, G., Kafkafi, N. & Golani, I. Controlling the false discovery rate in behavior genetics research. *Behav. Brain Res.* **125**, 279–284 (2001).
44. O'Geen, H., Frietze, S. & Farnham, P. J. Using ChIP–seq technology to identify targets of zinc finger transcription factors. *Methods Mol. Biol.* **649**, 437–455 (2010).
45. Li, R. et al. SOAP2: an improved ultrafast tool for short read alignment. *Bioinformatics* **25**, 1966–1967 (2009).
46. Lu, Z. et al. Genome-wide binding analysis of the transcription activator ideal plant architecture1 reveals a complex network regulating rice plant architecture. *Plant Cell* **25**, 3743–3759 (2013).
47. Wang, S. et al. The Os*SPL16-GW7* regulatory module determines grain shape and simultaneously improves rice yield and grain quality. *Nat. Genet.* **47**, 949–954 (2015).
48. Ho, C. H., Lin, S. H., Hu, H. C. & Tsay, Y. F. CHL1 functions as a nitrate sensor in plants. *Cell* **138**, 1184–1194 (2009).
49. Loqué, D. et al. Additive contribution of AMT1;1 and AMT1;3 to high-affinity ammonium uptake across the plasma membrane of nitrogen-deficient *Arabidopsis* roots. *Plant J.* **48**, 522–534 (2006).

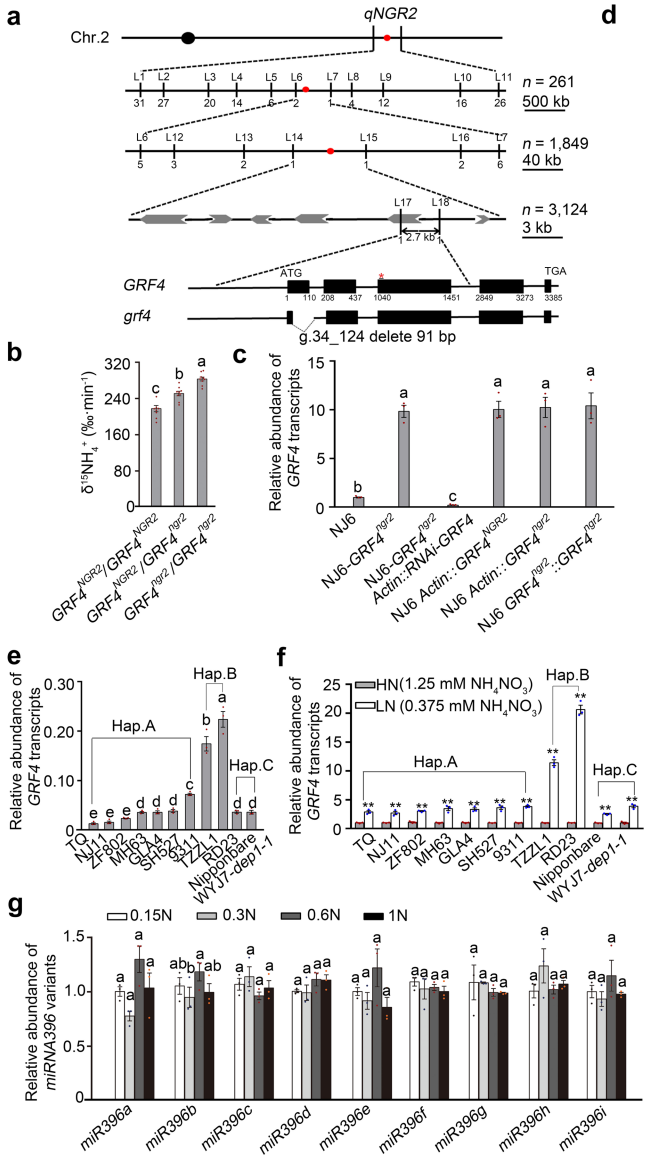

d

Haplotype	Hap.A	Hap.B	Hap.B	Hap.B	Hap.A	Hap.A	Hap.A	Hap.A	Hap.A	Hap.A	Hap.A	Hap.A	Hap.C	Hap.C
Position	NJ6 *GRF4*^{NGR2}	NM73 *GRF4*^{ngr2}	RD23	TZZL1	EJF	9311	HJX74	SH527	MH63	ZF802	NJ11	TQ	Nipponbare	WYJ7-*dep1-1*
-1008	G	G	G	G	G	G	G	G	G	G	G	G	A	A
-941	T	T	C	C	T	T	T	T	T	T	T	T	T	T
-884	T	A	A	A	T	T	T	T	T	T	T	T	T	T
-855	C	T	C	C	C	C	C	C	C	C	C	C	C	C
-847	C	T	T	T	C	C	C	C	C	C	C	C	C	C
-839	C	C	T	T	C	C	C	C	C	C	C	C	T	T
-818	T	T	C	C	T	T	T	T	T	T	T	T	C	C
-801	C	T	T	T	C	C	C	C	C	C	C	C	C	C
-792	A	A	A	A	A	A	A	A	A	A	A	A	G	G
-780	A	A	C	C	A	A	A	A	A	A	A	A	C	C
-558	C	C	–	–	C	C	C	C	C	C	C	C	A	A
-535	T	T	T	T	T	T	T	T	T	T	T	T	C	C
-522	C	T	C	C	C	C	C	C	C	C	C	C	C	C
-502	T	C	T	T	T	T	T	T	C	C	C	T	C	C
-357	G	G	G	G	G	G	G	G	G	G	G	G	-	-
-356	A	A	A	A	A	A	A	A	A	A	A	A	-	-
-355	G	G	G	G	G	G	G	G	G	G	G	G	-	-
-354	A	A	A	A	A	A	A	A	A	A	A	A	-	-
-353	G	G	G	G	G	G	G	G	G	G	G	G	-	-
-352	A	A	A	A	A	A	A	A	A	A	A	A	-	-
-324	G	A	G	G	A	G	G	G	G	G	G	A	G	G
-314	A	A	A	A	A	G	A	A	A	A	A	A	A	A
-309	T	T	A	A	A	A	T	T	A	A	T	T	A	A
-308	C	C	C	C	G	G	G	G	C	C	C	C	C	C
-188	C	C	C	C	C	C	C	C	C	C	C	C	G	G
-157	G	C	G	G	G	G	G	G	G	G	G	G	G	G
4	A	A	A	A	A	A	A	A	A	A	A	A	G	G
219	T	T	T	T	T	T	T	T	T	T	T	T	G	G
220	T	T	T	T	T	T	T	T	T	T	T	T	C	C
512	C	C	T	T	C	C	C	C	C	C	C	C	C	C
609	G	G	-	-	G	G	G	G	-	G	G	G	G	G
610	T	T	-	-	T	T	T	T	-	T	T	T	T	T
612	-	T	-	-	-	-	-	-	-	-	-	-	T	T
640	T	T	T	T	C	T	T	T	T	C	C	C	A	A
708	A	G	G	G	G	G	G	G	G	G	G	G	T	T
725	A	G	G	G	A	A	A	A	A	A	A	A	A	A
1187	T	A	T	T	T	T	T	T	T	T	T	T	T	T
1188	C	A	C	C	C	C	C	C	C	C	C	C	C	C
1554	T	T	C	C	T	T	T	T	T	T	T	T	C	C
1608	T	T	T	T	T	T	T	T	T	T	T	T	A	A
1661	C	C	C	C	C	C	C	C	C	C	C	C	T	T
1672	T	C	C	C	T	T	T	T	T	T	T	T	T	T
2096	A	A	A	A	A	A	A	A	A	A	A	A	G	G
2992	T	T	T	T	T	T	T	T	T	T	T	T	G	G
3481	T	T	T	T	T	T	T	T	T	T	T	T	A	A

Extended Data Fig. 1 | Allelic variation at the *GRF4* locus affects *GRF4* mRNA abundance and root $^{15}NH_4^+$ uptake. a, Positional cloning indicates the equivalence of *GRF4* with *qNGR2* (nitrogen-mediated growth response 2). Successive maps show progressive narrowing of focus of *qNGR2* (red dot, using recombination break points and linked DNA markers) to an approximately 2.7-kb region on chromosome 2 flanked by molecular markers L17 and L18 and overlapping candidate gene LOC_02g47280 (also known as *GRF4*). The start ATG (nucleotide 1) and close TGA (nucleotide 3385) of *GRF4* are shown, together with the protein-coding DNA sequence (thick black bars). The target site for miR396 is indicated by an asterisk. The structure of a CRISPR–Cas9-generated *grf4* mutant 91-bp deletion allele spanning parts of exon 1 and intron 1 is shown. **b**, $^{15}NH_4^+$ uptake rates of roots of BC_2F_2 progeny (derived from a NJ6 × NM73 cross) homozygous or heterozygous for *GRF4*^{NGR2} or *GRF4*^{ngr2} grown in high nitrogen supply (1.25 mM NH_4NO_3). Data are mean ± s.e.m. ($n = 9$). Different letters denote significant differences ($P < 0.05$) from a Duncan's multiple range test. **c**, *GRF4* mRNA abundance in plants (genotypes as shown) relative to the abundance in NJ6 (set to one). Data are mean ± s.e.m. ($n = 3$). Different letters denote significant differences ($P < 0.05$) from a Duncan's multiple range test. **d**, Natural varietal *GRF4* allelic variation. Nucleotide position relative to the *GRF4* start ATG is shown in **a**. SNPs shared between varieties NM73, RD23 and TZZL1 are highlighted. Sequences representative of *GRF4* promoter haplotypes A, B and C (see main text) are shown. **e**, *GRF4* mRNA abundance in various rice varieties under the high nitrogen conditions (1.25 mM NH_4NO_3), *GRF4* promoter haplotypes are indicated. Abundance data are all relative to the abundance of rice *Actin2* mRNA. Data are mean ± s.e.m. ($n = 3$). Different letters denote significant differences ($P < 0.05$) from a Duncan's multiple range test. **f**, Comparisons of *GRF4* mRNA abundance in selected rice varieties grown in between high (HN, 1.25 mM NH_4NO_3) and low (LN, 0.375 mM NH_4NO_3) nitrogen conditions. Data are mean ± s.e.m. ($n = 3$). Abundance data are all relative to the high nitrogen condition (set to one). $^{**}P < 0.05$ compared to high nitrogen in a two-sided Student's *t*-test. **g**, Relative abundances of rice miR396 family members in NJ6 plants grown at different levels of nitrogen supply (0.15N, 0.1875 mM NH_4NO_3; 0.3N, 0.375 mM NH_4NO_3; 0.6N, 0.75 mM NH_4NO_3; 1N, 1.25 mM NH_4NO_3), shown relative to the abundance in plants grown in 1N conditions (set to one). Data are mean ± s.e.m. ($n = 3$). Different letters denote significant differences ($P < 0.05$) from a Duncan's multiple range test.

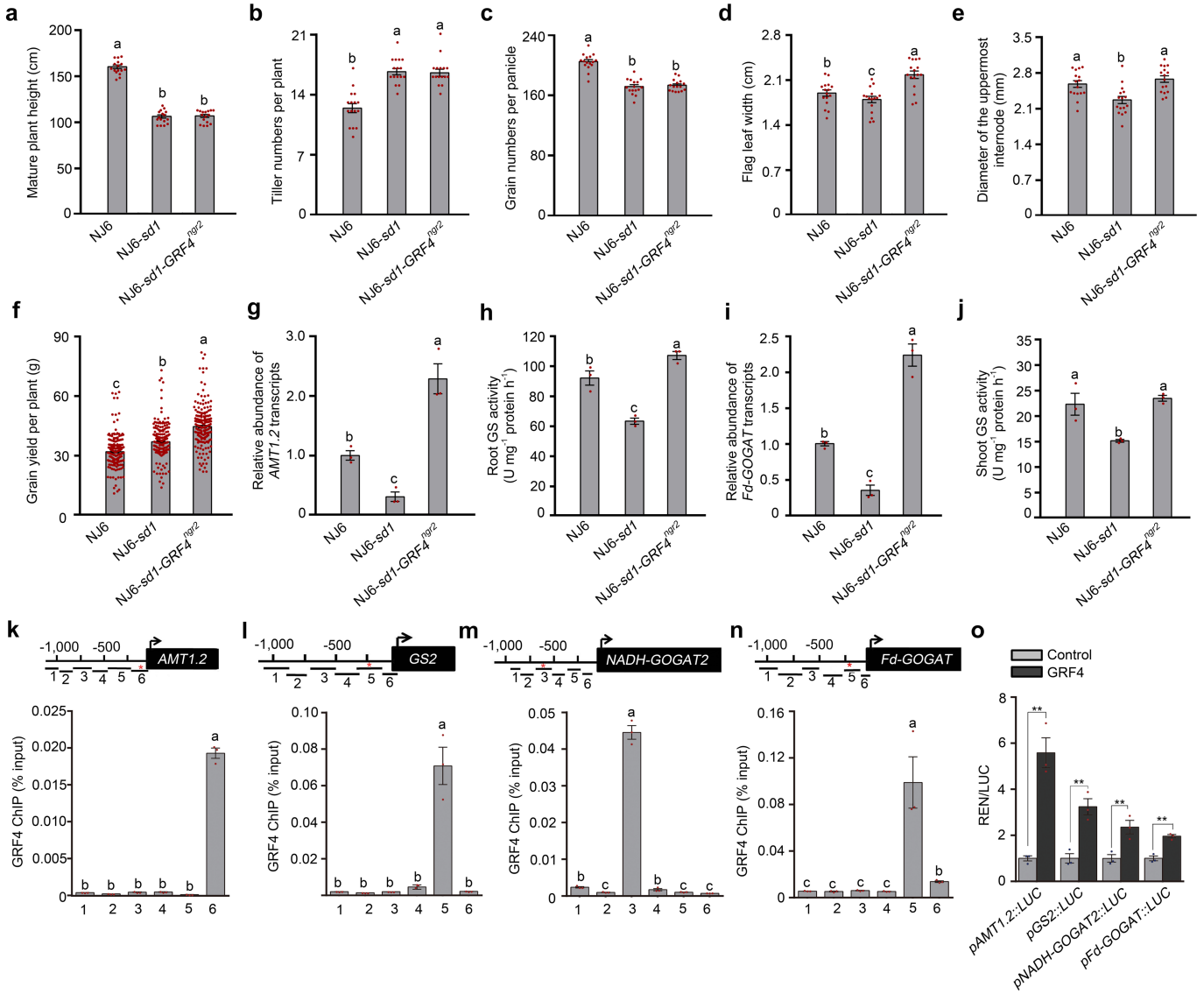

Extended Data Fig. 2 | Comparisons NJ6, NJ6-*sd1* and NJ6-*sd1-GRF4*^{ngr2} isogenic line traits reveals that GRF4 regulates expression of NH_4^+-metabolism genes. a, Mature plant height. Data are mean ± s.e.m. ($n = 16$). **b**, The number of tillers per plant. Data are mean ± s.e.m. ($n = 16$). **c**, The number of grains per panicle. Data are mean ± s.e.m. ($n = 16$). **d**, Flag-leaf width. Data are mean ± s.e.m. ($n = 16$). **e**, Culm (stem) width expressed as diameter of the uppermost internode. Data are mean ± s.e.m. ($n = 16$). **f**, Grain yield per plant. Data are mean ± s.e.m. ($n = 220$). **g**, Relative root abundance of *AMT1.2* mRNA in NILs, genotypes as indicated. Abundances shown are relative to NJ6 plants (set to 1). Data are mean ± s.e.m. ($n = 3$). **h**, Root glutamine synthase (GS) activities. Data are mean ± s.e.m. ($n = 3$). **i**, Relative shoot abundance of *Fd-GOGAT* mRNA. Abundances shown are relative to NJ6 plants (set to 1). Data are mean ± s.e.m. ($n = 3$). **j**, Shoot glutamine synthase (GS) activities. Data are mean ± s.e.m. ($n = 3$). **k–n**, Flag–GRF4-mediated ChIP–PCR enrichment (relative to input) of GCGG-containing promoter fragments (marked with an asterisk) from *AMT1.2*, *GS2*, *NADH-GOGAT2* and *Fd-GOGAT* promoters. Diagrams depict putative *AMT1.2*, *GS2*, *NADH-GOGAT2* and *Fd-GOGAT* promoters and fragments (1–6). Data are mean ± s.e.m. ($n = 3$; panels **k–n**). **a–n**, Different letters denote significant differences ($P < 0.05$) from a Duncan's multiple range test. **o**, GRF4 activates *AMT1.2*, *GS2*, *NADH-GOGAT2* and *Fd-GOGAT* promoter–luciferase fusion constructs in transient transactivation assays. Data are mean ± s.e.m. ($n = 3$). $^{**}P < 0.05$ compared to control group by two-sided Student's *t*-tests.

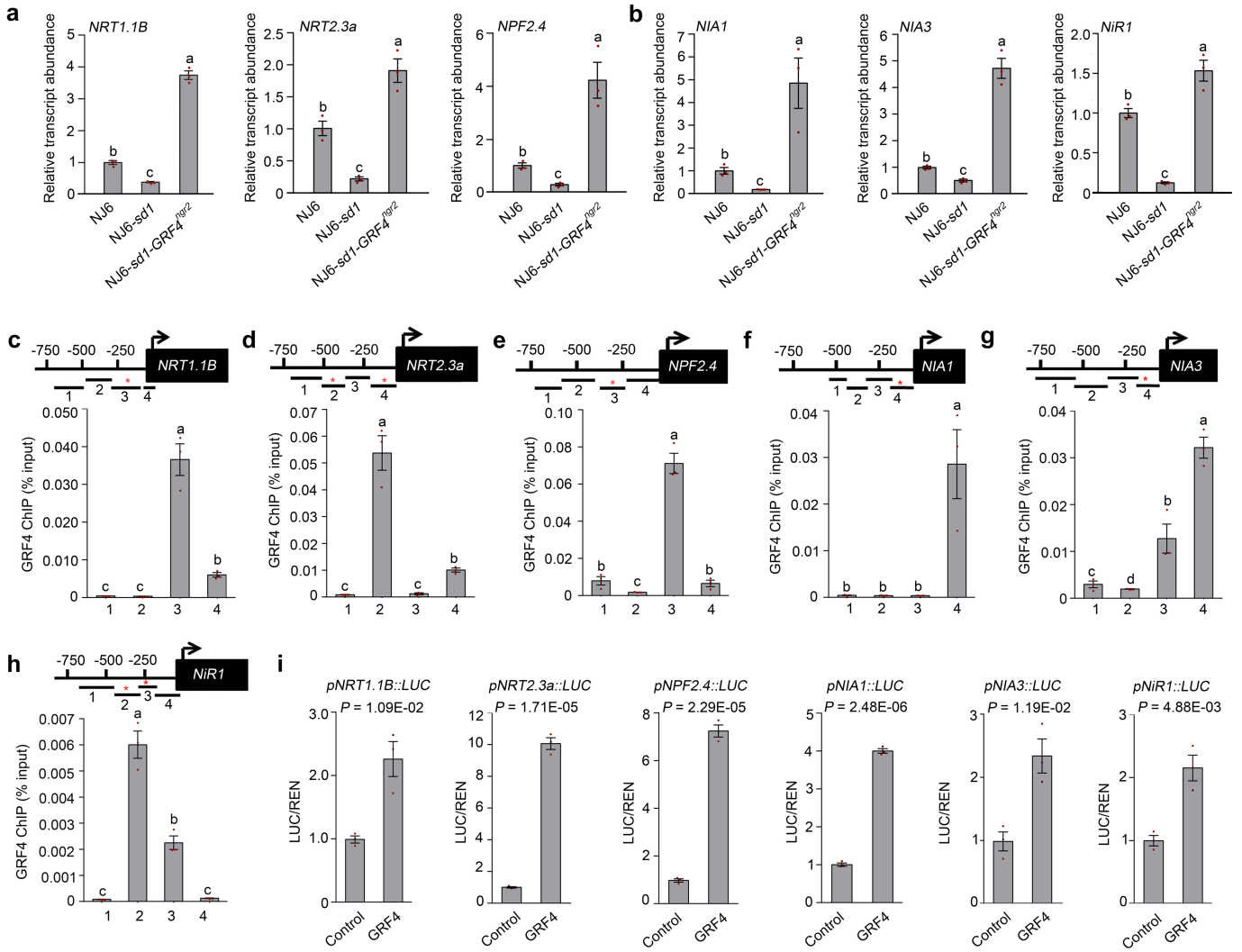

Extended Data Fig. 3 | GRF4 regulates expression of multiple NO_3^- metabolism genes. a, Relative abundance of *NRT1.1B*, *NRT2.3a* and *NPF2.4* mRNAs that encode NO_3^- uptake transporters. Abundances shown are relative to NJ6 (set to 1). Data are mean ± s.e.m. ($n = 3$). **b**, Relative abundances of *NIA1*, *NIA3* and *NiR1* mRNAs that encode NO_3^--assimilation enzymes. Abundances shown are relative to NJ6 (set to 1). Data are mean ± s.e.m. ($n = 3$). **c**–**h**, Flag–GRF4-mediated ChIP–PCR enrichment (relative to input) of GCGG-containing fragments (marked with asterisks) from promoters of *NRT1.1B* (**c**), *NRT2.3a* (**d**) and *NPF2.4* (**e**) genes that encode NO_3^--uptake transporters and *NIA1* (**f**), *NIA3* (**g**) and *NiR1* (**h**) genes that encode NO_3^--assimilation enzymes. Data are mean ± s.e.m. ($n = 3$). **a**–**h**, Different letters denote significant differences ($P < 0.05$) from a Duncan's multiple range test. **i**, GRF4 activates *NRT1.1B*, *NRT2.3a*, *NPF2.4*, *NIA1*, *NIA3* and *NiR1* promoter–luciferase fusion constructs in transient transactivation assays. Data are mean ± s.e.m. ($n = 3$) in all panels. *P* values are from a two-sided Student's *t*-test.

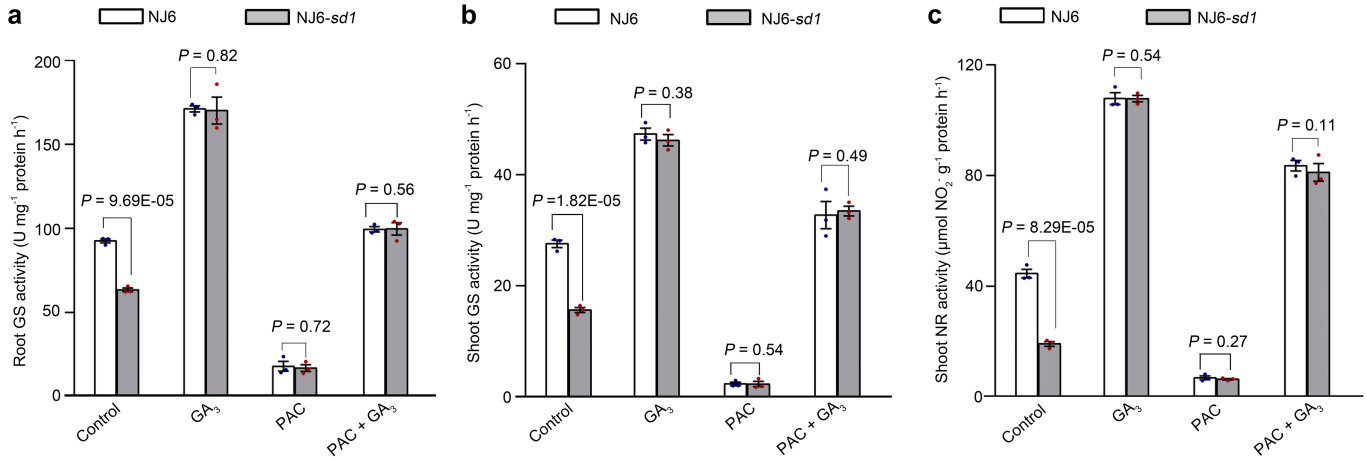

Extended Data Fig. 4 | GA promotes glutamine synthase and nitrate reductase activities. a, Glutamine synthase activities in roots of two-week-old rice plants treated with 100 μM GA (GA_3) and/or 2 μM PAC, genotypes as indicated. **b**, Glutamine synthase activities in shoots of plants treated with GA and/or PAC, genotypes and treatments as indicated in **a**. **c**, Nitrate reductase activities in shoots of plants treated with GA and/or PAC, genotypes and treatments as indicated in **a**. **a**–**c**, Data are mean ± s.e.m. ($n = 3$); *P* values are from two-sided Student's *t*-tests.

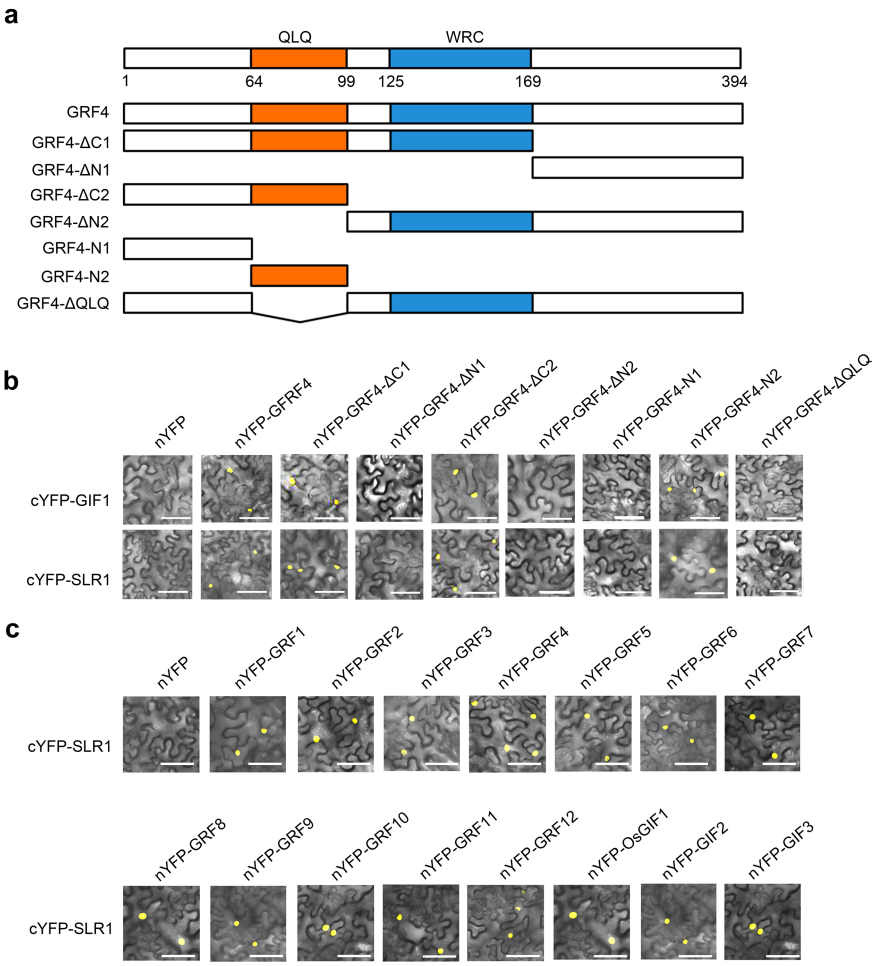

Extended Data Fig. 5 | BiFC visualization of SLR1–GIF1–GRF4 interactions. a, Details of constructs expressing GRF4 and variants deleted for specific domains. GRF4 contains the QLQ and WRC domains, positions as indicated. **b**, BiFC assays. Constructs expressing GRF4 or deletion variants (shown as in **a**) tagged with the N terminus of YFP were co-transformed into tobacco leaf epidermal cells, together with constructs expressing GIF1 or SLR1 tagged with the C terminus of YFP, respectively. Scale bars, 60 μm. **c**, BiFC assays. Constructs expressing GRF1 or related GRFs and GIFs family proteins tagged with the N terminus of YFP were co-transformed into tobacco leaf epidermal cells together with a construct expressing SLR1 tagged with the C terminus of YFP. Scale bar, 60 μm. **b**, **c**, Images of BiFC assays are representative of three experiments performed independently with similar results.

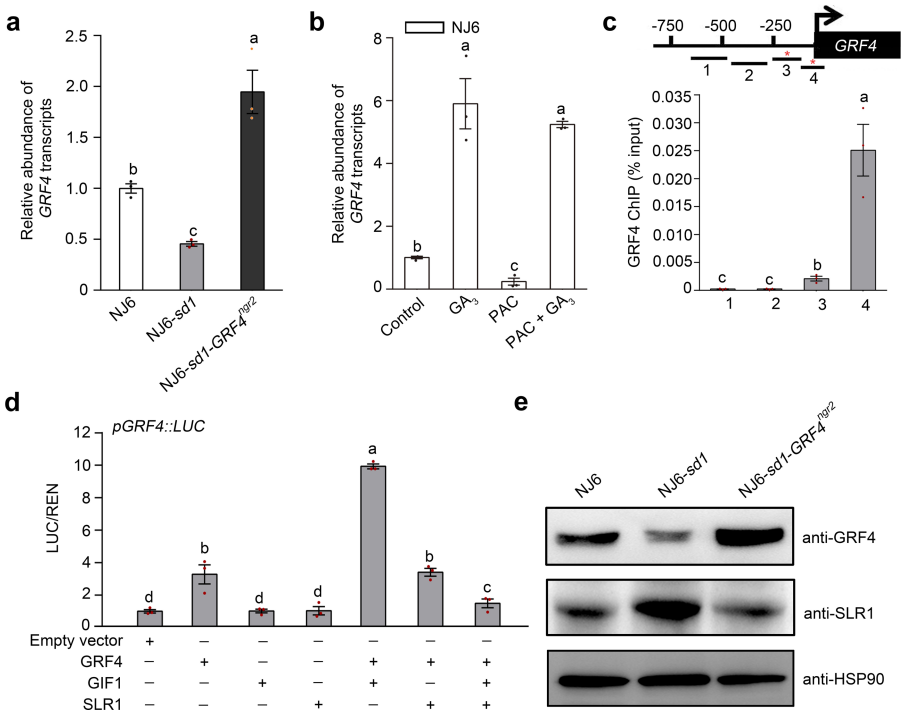

Extended Data Fig. 6 | SLR1 inhibits GRF4–GIF1 self-promotion of *GRF4* mRNA and GRF4 protein abundance. a, *GFR4* mRNA abundance, plant genotypes as indicated. Abundances shown are relative to NJ6 (set to 1). **b**, The effects of GA and PAC on *GRF4* mRNA abundance in two-week-old NJ6 plants. Abundances shown are relative to the water treatment control (set to 1). **c**, ChIP–PCR GRF4-mediated enrichment (relative to input) of GCGG-containing *GRF4* promoter fragments (marked with asterisks). **d**, GRF4-activated promotion of transcription from the *GRF4* gene promoter-luciferase reporter construct is enhanced by GIF1 and inhibited by SLR1. Luciferase/renilla activity shown relative to the empty vector control (set to 1). **a**–**d**, Data are mean ± s.e.m. ($n = 3$). Different letters denote significant differences ($P < 0.05$) from Duncan's multiple range tests. **e**, GRF4 abundance (as detected by an anti-GRF4 antibody), plant genotypes as indicated. HSP90 serves as loading control. Blots are representative of three experiments performed independently with similar results.

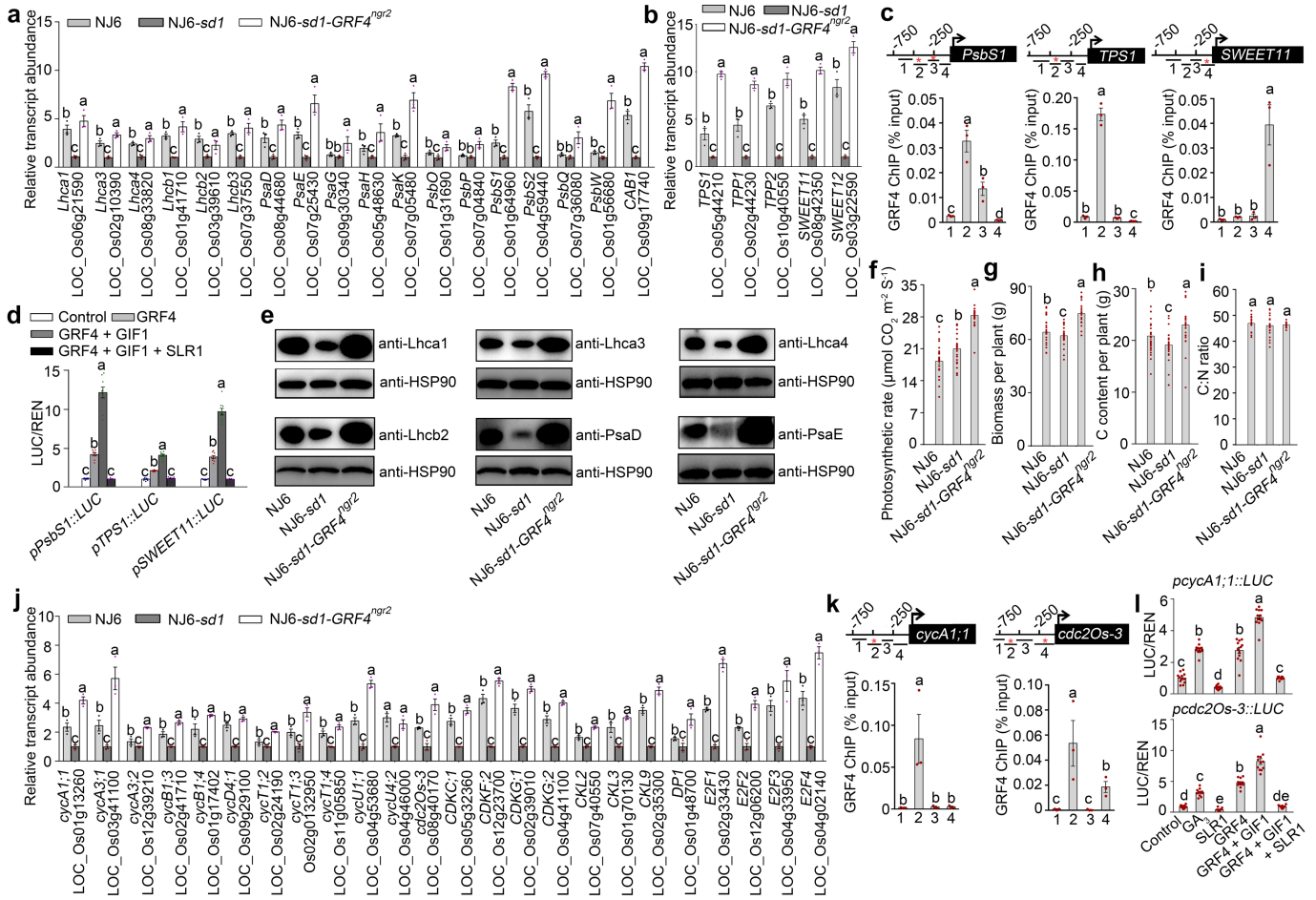

Extended Data Fig. 7 | The GRF4–SLR1 antagonism regulates carbon assimilation and plant growth. a, **b**, Relative shoot abundances of carbon-fixation gene mRNAs. Abundances of transcripts of genes regulating photosynthesis (**a**), sucrose metabolism and transport/phloem loading (**b**) in NJ6, NJ6-*sd1* and NJ6-*sd1-GRF4*^{ngr2} plants. Abundances in NJ6 and NJ6-*sd1-GRF4*^{ngr2} are expressed relative to NJ6-*sd1* (set to 1). **c**, ChIP–PCR assays. Diagrams depict the *PsbS1*, *TPS1* and *SWEET11* promoters and regions used for ChIP–PCR, and GCGG-containing promoter fragment (marked with asterisks) enrichment (relative to input). **a**–**c**, Data are mean ± s.e.m. ($n = 3$). **d**, Transactivation assays. The luciferase/renilla activity obtained from a co-transfection with an empty effector construct and indicated reporter constructs was set to 1. Data are mean ± s.e.m. ($n = 9$). **e**, Immunoblot detection of Lhca1, Lhca3, Lhca4, Lhcb2, PsaD and PsaE using antibodies as shown in genotypes as indicated. HSP90 serves as loading control. Blots are representative of three experiments performed independently with similar results. **f**–**i**, Comparisons of photosynthetic rates (**f**), biomass (**g**), carbon content (**h**) and C:N ratio (**i**) in NJ6, NJ6-*sd1* and NJ6-*sd1-GRF4*^{ngr2} plants. Data are mean ± s.e.m. ($n = 30$). **j**, Relative shoot abundances of mRNAs transcribed from cell-cycle regulatory genes in NJ6, NJ6-*sd1* and NJ6-*sd1-GFR4*^{ngr2} plants. Transcription is relative to NJ6-*sd1* plants (set to 1). Data are mean ± s.e.m. ($n = 3$). **k**, ChIP–PCR assays. Diagrams depict the *cycA1.1* and *cdc2Os-3* promoters and regions (GCGG-containing fragment marked with asterisks) used for ChIP–PCR. Data are mean ± s.e.m. ($n = 3$). **l**, Transactivation assays from the *cycA1.1*and *cdc2Os-3* promoters. Data are mean ± s.e.m. ($n = 12$). **a**–**d**, **f**–**l**, Different letters denote significant differences ($P < 0.05$) from Duncan's multiple range tests.

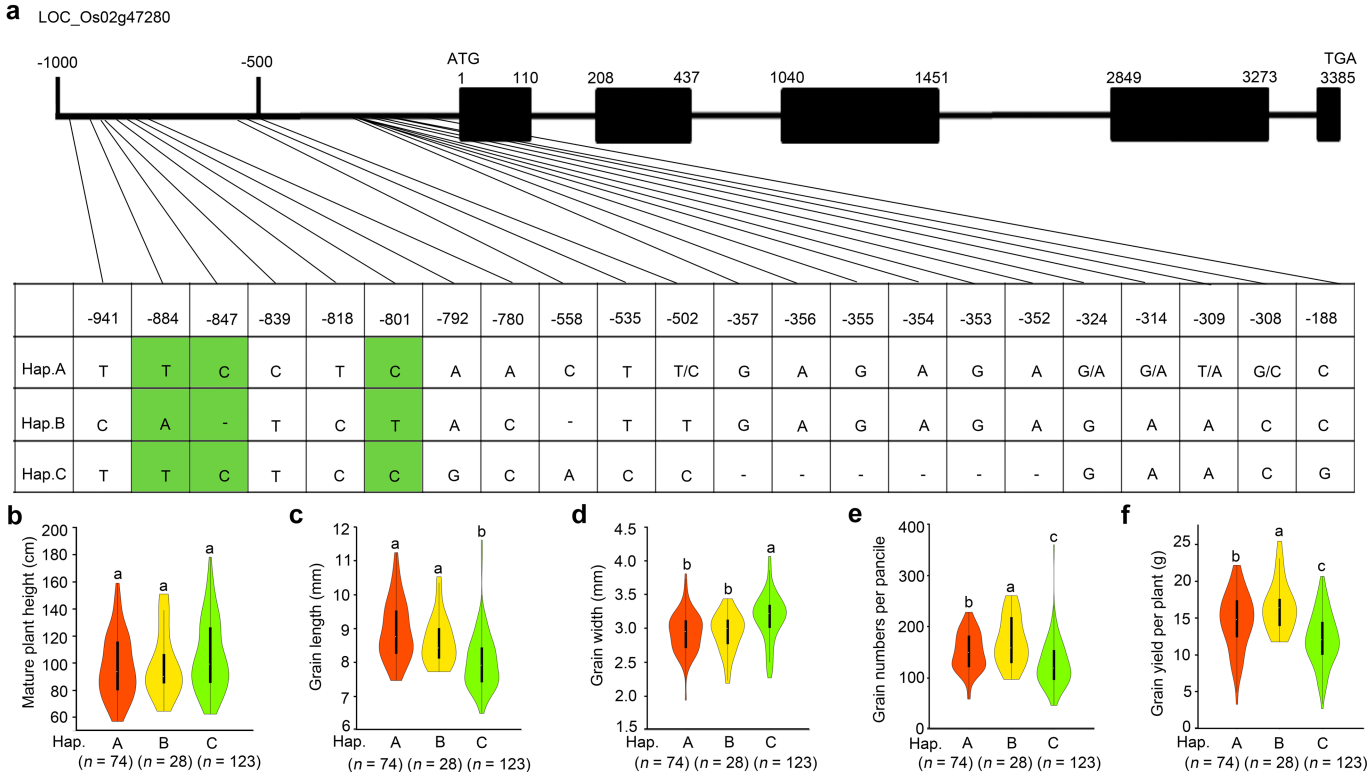

	-941	-884	-847	-839	-818	-801	-792	-780	-558	-535	-502	-357	-356	-355	-354	-353	-352	-324	-314	-309	-308	-188
Hap.A	T	T	C	C	T	C	A	A	C	T	T/C	G	A	G	A	G	A	G/A	G/A	T/A	G/C	C
Hap.B	C	A	-	T	C	T	A	C	-	T	T	G	A	G	A	G	A	G	A	A	C	C
Hap.C	T	T	C	T	C	C	G	C	A	C	C	-	-	-	-	-	-	G	A	A	C	G

Extended Data Fig. 8 | Natural allelic variation at *GRF4* is associated with variation in plant and grain morphology and grain yield performance. a, DNA polymorphisms in the promoter region of *GRF4*. Green-shaded regions indicate the three unique SNP variations associated with phenotypic variation in NM73 and RD23. **b–f**, Box plots for plant height (**b**), grain length (**c**), grain width (**d**), the number of grains per panicle (**e**) and grain yield performance (**f**) of rice varieties carrying different *GRF4* promoter haplotypes (Hap. A, B or C). All data are from plants grown under normal paddy-field fertilization conditions[22]. Data are mean ± s.e.m. (Hap. A, $n = 74$; Hap. B, $n = 28$; Hap. C, $n = 123$). The violin plot was constructed in R. **b–f**, Different letters indicate statistically significant differences between groups ($P < 0.05$) from a Tukey's honestly significant difference (HSD) test.

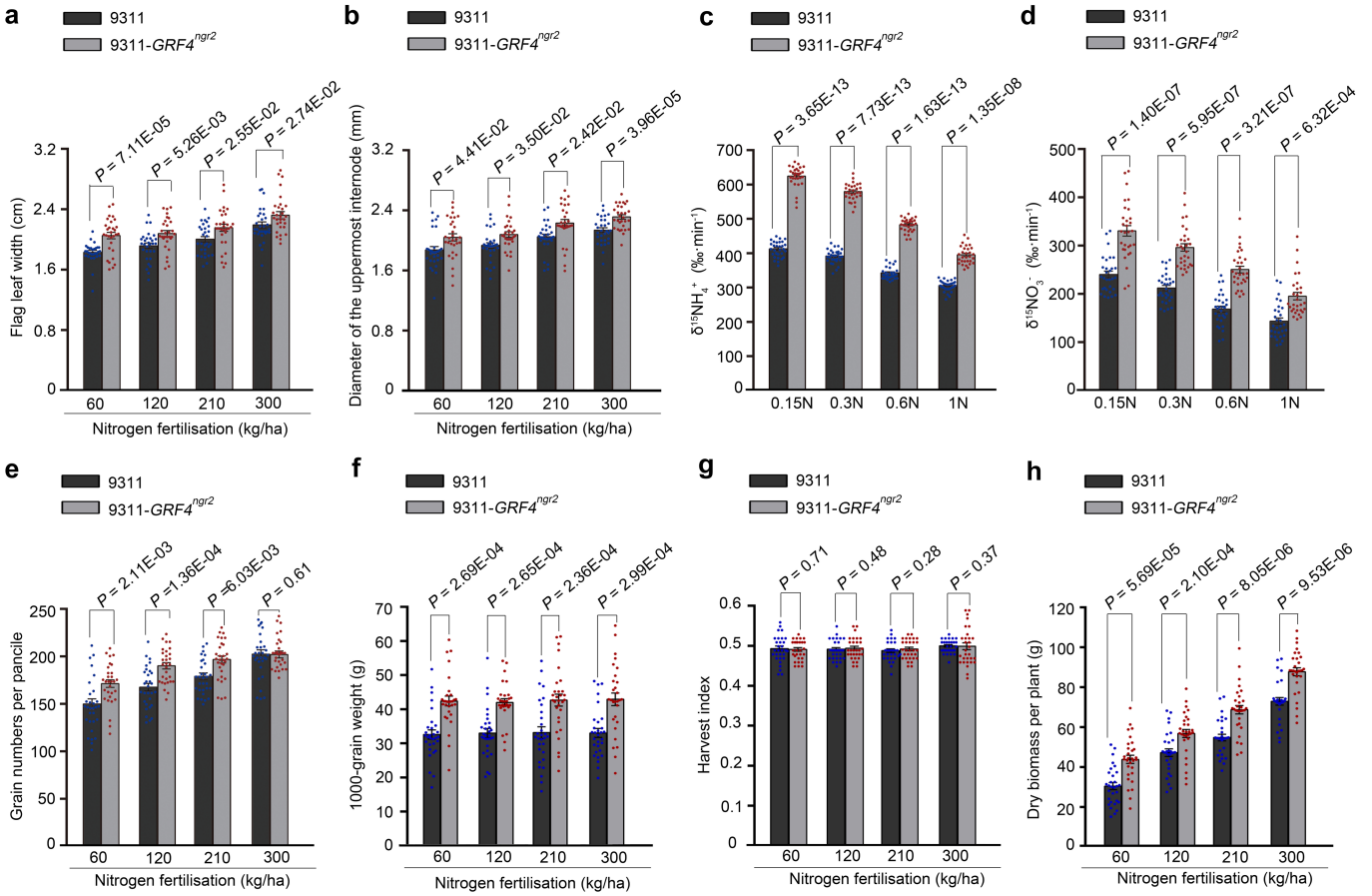

Extended Data Fig. 9 | Agronomic traits displayed by 9311 and 9311-*GRF4*^{ngr2} plants grown at varying nitrogen fertilization levels. **a**, **b**, Flag leaf width (**a**) and culm width of the uppermost internode (**b**) at varying levels of nitrogen fertilization. **c**, **d**, $^{15}NH_4^+$ (**c**) and $^{15}NO_3^-$ (**d**) uptake rates of four-week-old plants grown with varying nitrogen supply (0.15N, 0.1875 mM NH_4NO_3; 0.3N, 0.375 mM NH_4NO_3; 0.6N, 0.75 mM NH_4NO_3; 1N, 1.25 mM NH_4NO_3). **e**–**h**, The number of grains per panicle (**e**), 1,000-grain weight (**f**), harvest index (**g**) and dry biomass per plant (**h**) at varying levels of nitrogen fertilization. **a**–**h**, Data are mean ± s.e.m. ($n = 30$); *P* values are from two-sided Student's *t*-tests.

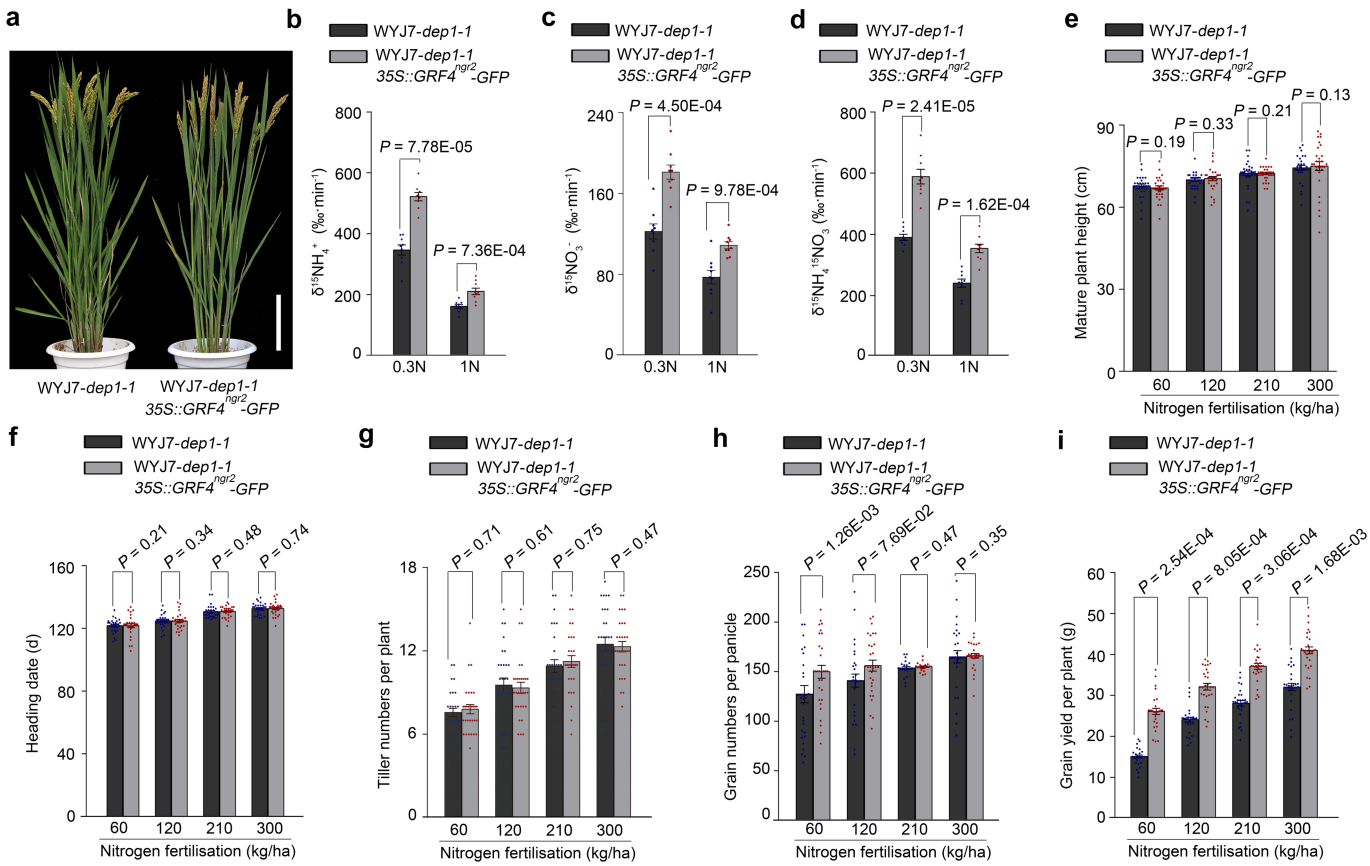

Extended Data Fig. 10 | Growth, nitrogen uptake and grain yield performance of WYJ7-*dep1-1* and transgenic WYJ7-*dep1-1* plants carrying the *35S::GRF4^{ngr2}–GFP* construct at varying levels of nitrogen fertilization. a, Mature plant heights. Scale bar, 15 cm. The picture is representative of three experiments performed independently with similar results. **b**–**d**, Root uptake rates for $^{15}NH_4^+$ (**b**), $^{15}NO_3^-$ (**c**), and $^{15}NH_4^+$ and $^{15}NO_3^-$ combined (**d**) of four-week-old rice plants grown in low nitrogen (0.3N, 0.375 mM NH_4NO_3) and high nitrogen (1N, 1.25 mM NH_4NO_3) conditions. Data are mean ± s.e.m. ($n = 9$). **e**–**i**, Mature plant height (**e**), heading date (**f**), the number of tillers per plant (**g**), the number of grains per panicle (**h**) and grain yield per plant (**i**) at varying levels of nitrogen fertilization. **e**–**i**, Data shown as mean ± s.e.m. ($n = 30$). **b**–**i**, *P* values are from two-sided Student's *t*-tests.

nature research

Corresponding author(s): Xiangdong Fu

Reporting Summary

Nature Research wishes to improve the reproducibility of the work that we publish. This form provides structure for consistency and transparency in reporting. For further information on Nature Research policies, see Authors & Referees and the Editorial Policy Checklist.

Statistical parameters

When statistical analyses are reported, confirm that the following items are present in the relevant location (e.g. figure legend, table legend, main text, or Methods section).

n/a	Confirmed	
☐	☒	The exact sample size (*n*) for each experimental group/condition, given as a discrete number and unit of measurement
☐	☒	An indication of whether measurements were taken from distinct samples or whether the same sample was measured repeatedly
☐	☒	The statistical test(s) used AND whether they are one- or two-sided *Only common tests should be described solely by name; describe more complex techniques in the Methods section.*
☐	☒	A description of all covariates tested
☐	☒	A description of any assumptions or corrections, such as tests of normality and adjustment for multiple comparisons
☐	☒	A full description of the statistics including central tendency (e.g. means) or other basic estimates (e.g. regression coefficient) AND variation (e.g. standard deviation) or associated estimates of uncertainty (e.g. confidence intervals)
☐	☒	For null hypothesis testing, the test statistic (e.g. *F*, *t*, *r*) with confidence intervals, effect sizes, degrees of freedom and *P* value noted *Give P values as exact values whenever suitable.*
☒	☐	For Bayesian analysis, information on the choice of priors and Markov chain Monte Carlo settings
☐	☒	For hierarchical and complex designs, identification of the appropriate level for tests and full reporting of outcomes
☐	☒	Estimates of effect sizes (e.g. Cohen's *d*, Pearson's *r*), indicating how they were calculated
☐	☒	Clearly defined error bars *State explicitly what error bars represent (e.g. SD, SE, CI)*

Our web collection on statistics for biologists may be useful.

Software and code

Policy information about availability of computer code

Data collection	Sequencing reads were undertaken with the BGISEQ-500 sequencer.
Data analysis	SigmaPlot v11, SPSS v18.0, GraphPad Prism, HISAT40, Bowtie2, RESM, SOAP aligner/soap2, Burrows-Wheeler Aligner and IGV2.3.91 statistical softwares were used for statistical analysis.

For manuscripts utilizing custom algorithms or software that are central to the research but not yet described in published literature, software must be made available to editors/reviewers upon request. We strongly encourage code deposition in a community repository (e.g. GitHub). See the Nature Research guidelines for submitting code & software for further information.

Data

Policy information about availability of data

All manuscripts must include a data availability statement. This statement should provide the following information, where applicable:

- Accession codes, unique identifiers, or web links for publicly available datasets
- A list of figures that have associated raw data
- A description of any restrictions on data availability

We have included a data availability statement in the revised version of the manuscript. The ChIP-seq data sets generated have been deposited in the Gene Expression Omnibus (GEO) under accession GSE114287.

Field-specific reporting

Please select the best fit for your research. If you are not sure, read the appropriate sections before making your selection.

☒ Life sciences ☐ Behavioural & social sciences ☐ Ecological, evolutionary & environmental sciences

For a reference copy of the document with all sections, see nature.com/authors/policies/ReportingSummary-flat.pdf

Life sciences study design

All studies must disclose on these points even when the disclosure is negative.

Sample size	Required experimental sample sizes were estimated based on our past experience performing similar experiments including field test.
Data exclusions	The results were excluded from the analysis if the positive control experiments were not successful.
Replication	All experiments were successfully repeated at least three times, and we have stated it in figure legends .
Randomization	Plants of equal initial sizes were randomly assigned to the treatment and control groups.
Blinding	Analysis were performed in a manner blinded to treatment assignment in all experiments.

Reporting for specific materials, systems and methods

Materials & experimental systems

n/a	Involved in the study
☒	☐ Unique biological materials
☐	☒ Antibodies
☒	☐ Eukaryotic cell lines
☒	☐ Palaeontology
☒	☐ Animals and other organisms
☒	☐ Human research participants

Methods

n/a	Involved in the study
☐	☒ ChIP-seq
☒	☐ Flow cytometry
☒	☐ MRI-based neuroimaging

Antibodies

Antibodies used	anti-Flag antibodies (Sigma, F1804, Lot No. # SLBN5629V, 1:5000), anti-OsGRF4 antibodies (Abmart, 1:2000), anti-SLR1 antibodies (ABclonal Technology, 1:2000), anti-OsLhca1 antibodies (Agrisera, AS01005, Lot No.1703, 1:5000), anti-OsLhca3 antibodies (Agrisera, AS01007, Lot No.1309, 1:5000), anti-OsLhca4 antibodies (Agrisera, AS01008, Lot No.1405 , 1:5000), anti-OsLhcb2 antibodies (Agrisera, AS01003, Lot No.1711, 1:5000), anti-OsPsaD antibodies (Agrisera, AS09461, Lot No.1309, 1:1000) , anti-OsPsaE antibodies (Agrisera, AS08324A, 1:1000), anti-HSP antibodies (BGI, AbM51099-31-PU, Lot No. 2017122801, 1:10000), anti-DDDDK-tag antibodies (MBL, M185-11, Lot No. 006, 1: 5000), and anti-HA antibodies (MBL, M180-7, Lot No. 004, 1: 5000).
Validation	anti-Flag antibodies (The ANTI-FLAG M2 mouse, affinity purified monoclonal antibody binds to fusion proteins containing a FLAG peptide sequence.The antibody recognizes the FLAG peptide sequence at the N-terminus, Met-N-terminus,C-terminus, and internal sites of the fusion protein.). anti-OsLhca1 antibodies, anti-OsLhca3 antibodies, anti-OsLhca4 antibodies and anti-OsLhcb2 antibodies (Reactivity: antibodies have been shown to be reactive in all dicots, monocots, and gymnosperms tested so far; some of them have even been found to be reactive against Lhc-proteins of Chlamydomonas reinhardtii). anti-OsPsaD antibodies (Confirmed reactivity: Arabidopsis thaliana, Chlamydomonas reinhardtii, Hordeum vulgare, Lactuca sativa, Oryza sativa, Physcomitrella patens, Spinacia oleracea, Synechocystis PCC 6803, Triticum aestivum, Zea mays; Predicted reactivity: plants (monocots, dicots and conifers), Bigelowiella natans, Cucumis melo, green algae). anti-OsPsaE antibodies (Confirmed reactivity: Arabidopsis thaliana; Predicted reactivity: dicots including Spinacia oleracea, monocots including: Hordeum vulgare, Oryza sativa, Zea mays, trees: Populus canadensis, algae: Chlamydomonas reinhardtii, Chlorella). anti-HSP antidodies (Reactivity: This antibody reacts with house-keeping gene HSP in rice). anti-DDDDK-tag antibodies (Reactivity: This antibody reacts with N-terminal, Internal and C-terminal DDDDK-tagged (DYKDDDDK) protein). anti-HA antibodies (Reactivity: This antibody reacts with N-terminal and C-terminal tagged protein). Loss-of-function mutants (e.g., osgrf4 mutant) were used to validate anti-OsGRF4 antibodies. Loss-of-function mutants (e.g., slr mutant) were used to validate anti-SLR1 antibodies.

ChIP-seq

Data deposition

☒ Confirm that both raw and final processed data have been deposited in a public database such as GEO.

☒ Confirm that you have deposited or provided access to graph files (e.g. BED files) for the called peaks.

Data access links *May remain private before publication.*	https://www.ncbi.nlm.nih.gov/geo/query/acc.cgi?acc=GSE114287 The following secure of record GSE114287 for reviewer while it remains in private status is yridcccmxbkjlcx.
Files in database submission	Input3.fastq, Flag3.fastg, Input4.fastq, Flag4.fastq, LH93-Input.fastq, LH93-Flag.fastq, LH93.bed, Flag3.bed, Flag4.bed
Genome browser session (e.g. UCSC)	http://ensembl.gramene.org/Oryza_sativa/Info/Index

Methodology

Replicates	Three biological repeat samples were mixed together
Sequencing depth	Average tag depth of Flag3 is 294. Average tag depth of Flag4 is 200. Average tag depth of LH93-Flag is 231.
Antibodies	anti-Flag antibodies (Sigma, F1804).
Peak calling parameters	Peak calling parameters ：-s 50 -g 380000000 -p 1e-5 -w --space 50 -m 10,30
Data quality	Clean Parameter: SOAPnuke filter -l 5 -q 0.5 -n 0.1 -Q 2 -c 25
Software	BGISEQ-500, SOAPaligner/SOAP2, Burrows-Wheeler Aligner, Model-based Analysis of ChIP -Seq, IGV2.3.91